Integrated Master in Chemical Engineering

Diffusion measurements in liquid mixtures by Raman spectroscopy

Master Thesis

Developed for the course

Development Project in a Foreign Institution

José Fernandes

LAPPEENRANTA
UNIVERSITY OF TECHNOLOGY

Universidade do Porto
Faculdade de Engenharia
FEUP

Department of Chemical Technology

Chemical Engineer Department

Graduating Professor: **Professor Marjatta Louhi-Kultanen**

Supervisor: **MSc. Sanna Ojanen**

Evaluator in the home institution**: Professor Alexandra Rodrigues Pinto**

August 2009

Acknowledgments

To the Lappeenranta University of Technology (LUT) and to the Laboratory of Chemical Engineering, in the person of Professor of Marjatta Louhi-Kultanen for having provided the facilities and technical conditions needed to perform this work.

I thank my supervisor, Professor Marjatta Louhi-Kultanen for her guidance, comments and constructive advices. Thank you, for having contributed for my scientific and personal growth and having provided me the opportunity to perform this work.

I deeply express my eternal gratitude to Sanna Ojanen for her friendship, encouragement, and help. Every-day, from the very first moment till the end of my stay, your guidance, your support, and your advices made my work successful.

I thanks to Professor Alexandra Pinto for having accepted and evaluated my thesis. Thanks also to Professor Miguel Madeira and Professor João Campos for their understanding, help and support that made possible my stay in Finland within ERASMUS program.

I thank Professor Heikki Haario for his precious help with the implementation of the mathematical model. Thanks also to Haiyan Qu for her valuable comments and suggestions regarding the instrumentation.

I want to thank the all the wonderful persons who I meet in Lappeenranta, persons from different parts of the world with whom I had the privilege to share amazing moments in the unforgettable Lappeenranta.

Last, but definitely not the least, thanks to my parents, my brother and my family. A special thanks to my godmother, Filomena Barreiro, for having always encourage me.

To my friends who always believed in me.

Kiitos teille kaikille!

Abstract

Model-based Raman spectroscopy methodology is a recent technique that offers high potential to perform diffusion studies. In this work this methodology was tested at the Department of Chemical Technology at Lappeenranta University. The used experimental set-up includes a Horiba Jobin-Yvon LabRam 300 Raman microscope (equipped with liquid nitrogen cooled charge-coupled device (CCD) detector and a fiber optic probe) and a diffusion cell.

The experimental procedure comprising cell filling, calibration and diffusion measurements was tested with success using the binary liquid mixture ethanol+ethyl acetate. Data acquisition was done with the software LabSpec and the acquisition parameters have been optimized. In order to determine the composition of the mixture from the spectral data two different approaches have been used (peak height and peak area). The one based on peak height proved to be less influenced by Raman spectra noise and was the preferential method used in this work.

The obtained time-dependent concentration profiles fitted according with two approaches, the one based on the numerical resolution of the Fick's second law and the one based on its analytical solution (provided by Berg *et al*. [16]) proved to generate reliable diffusion coefficients. Furthermore, the obtained values are in agreement with the ones predicted by the predictive methods.

The diffusion coefficient of ethyl acetate in ethanol was estimated as 1.55×10^{-5} cm^2/s. The ethanol molar fraction interval from 0.5 to 0.7 (ethanol average composition of 0.6) generates the most accurate results, i.e. a better agreement with the values generated by the predictive models was observed.

The experimental set-up together with the methodology for data acquisition and treatment proved to be adequate for diffusion studies purposes and could be extended to other binary liquid mixtures or even multicomponent mixtures.

Key words: Diffusion coefficient, Model-based Raman spectroscopy, Binary liquid mixtures

Table of Contents

List of figures

List of tables

List of symbols and abbreviations

A	Area	m^2
a	Activity	Dimensionless
c	Concentration	mol kg^{-1}
D	Diffusion coefficient	m^2 s^{-1}
D^0	Diffusion coefficient at infinite dilution	m^2 s^{-1}
$Đ$	Maxwell-Stefan diffusion coefficient	m^2 s^{-1}
D_{12}	Mutual diffusion coefficient of solute 1 in solvent 2	m^2 s^{-1}
Da	Diffusion coefficient numerical solution	m^2 s^{-1}
Db	Diffusion coefficient analytical solution	m^2 s^{-1}
erf	Error function	Dimensionless
f	Friction coefficient of the solute	Dimensionless
G	Parameter of NRTL equation	Dimensionless
G_m	Molar Gibbs energy	J mol^{-1}
J	Mass flow rate	Kg s^{-1}
j	Flux per unit area	Kg m^{-2} s^{-1}
k_B	Boltzmann´s constant	J K^{-1}
M	Molecular weight	g mol^{-1}
m	Mass	kg
P	Pressure and parachors	Pa and Dimensionless
R	Gas constant	J K^{-1} mol^{-1}
R_0	Solute radius	m
T	Temperature	K
t	Time	s
$t_{injection}$	Injection time	s
u	Velocity	m s^{-1}
V	Volume	m^3
x	Molar fraction and wavenumber	Dimensionless and m^{-1}
y	Intensity	a.u.
z	Distance	m

Greek letters

$\zeta_{1,2}$	Friction coefficient between the components 1 and 2	Dimensionless
ψ_1	Total potential	J
γ	Activity coefficient	Dimensionless
μ	Chemical potential and solvent viscosity	J and Pa s
α	Thermodynamic correlation factor	Dimensionless
η	Viscosity	Pa s
ϕ	Wilke-Chang correlation constant	Dimensionless
σ	Surface tension	N m^{-1}
ρ	Specific gravity	m s^{-2}
Λ	Parameter of Wilson equation	Dimensionless
τ	Parameter of NRTL and Wilson equations	Dimensionless

Abbreviations

NMR	Nuclear Magnetic Resonance
HPLC	High Performance Liquid Chromatography
NRTL	Non-Random Two Liquid model
IR	Infrared
EPR	Electron Paramagnetic Resonance
UV	Ultraviolet
FT	Fourier Transform
CCD	Charge-Coupled Device

1 Introduction

Diffusion is a property by which gases or liquids mix spontaneously because of the random motion of their particles. Diffusion can arise from pressure gradients, temperature gradients, external force fields and concentration gradients. Diffusion is the rate-limiting step in many mass-transfer operations, such as distillation, extraction, absorption and chemical reaction in heterogeneous medium.

The available data on diffusion coefficients, even for binary mixtures, is scarce. Diffusion in liquids is a very slow process and experimental studies are in general characterized to be complex and time-consuming. Moreover, the determination of concentration dependence of diffusion coefficient needs several experiments.

Recently, a novel procedure to study diffusivity using model-based Raman spectroscopy was developed, being the pioneer groups the ones of Bardow [26, 28 and 29] and Berg [16]. This methodology can be used to obtain liquid concentration data of the mixture components simultaneously thus reducing the experimental effort for diffusion measurements.

The main objective of this work was the implementation of the model-based Raman spectroscopy to perform diffusion studies at the Department of Chemical Technology at Lappeenranta University of Technology. For that purpose an experimental set-up was tested and improved considering the following aspects: cell filling procedure and increasing laser power in order to reduce noise. Data acquisition and data treatment was performed and optimized. The methodology was used to determine the diffusion coefficient in the mixture ethanol-ethyl acetate in a wide concentration range. Previously to diffusion experiments the system was calibrated using the pure liquids (also used to define the characteristic Raman peaks – non-overlapping peaks) and solutions of different composition. The experimentally determined diffusion coefficient values were in agreement with the values estimated using predictive models.

The work is organized as follows:

Chapter 2 gives an insight into diffusive mass transfer. The importance of the phenomenon is depicted using practical examples. The fundamental laws of diffusion and its development and history are explained. The definition and determination (experimental and using predictive models) of the diffusion coefficients is presented. In the end of the chapter an overview of multicomponent diffusion is given.

In Chapter 3 the principles of Raman spectroscopy are explained in detail, as well as the Raman instrumentation. Diffusion measurements using Raman technique are presented in the end of the chapter. Previous works illustrate of the applicability of this technique towards diffusion study in liquids are reviewed.

Chapter 4 describes the experimental setup and the methodology used to perform the diffusion studies by Raman spectroscopy within this work. The mathematical data treatment and the diffusion models utilized are described. In the end of the chapter the predictive models used are presented.

In Chapter 5 the data obtained for the diffusion coefficient measurements are presented and discussed. In the absence of literature data, the experimentally determined values were evaluated using predictive models. Finally, the used Raman methodology is discussed.

The work ends with the main conclusions and perspectives of future work that are summarized in Chapter 6.

2 Diffusion

Diffusion is a phenomenon caused by random motion of individual molecules that leads to a complete mixing (Figure 2.1). The molecular motion is due to their kinetic energy and it causes random and irregular movements. Diffusion can arise from pressure gradients, temperature gradients, external force fields and concentration gradients [1]. It may be a slow process, i.e., in gases, the diffusion progression rate may be around 10 cm/min, in liquids its rate is considerable slower, about 0.05 cm/min and in solids, its rate can be only about 0.00001 cm/min. Diffusion in liquids, comparing with many other phenomena, does not vary significantly with temperature [2].

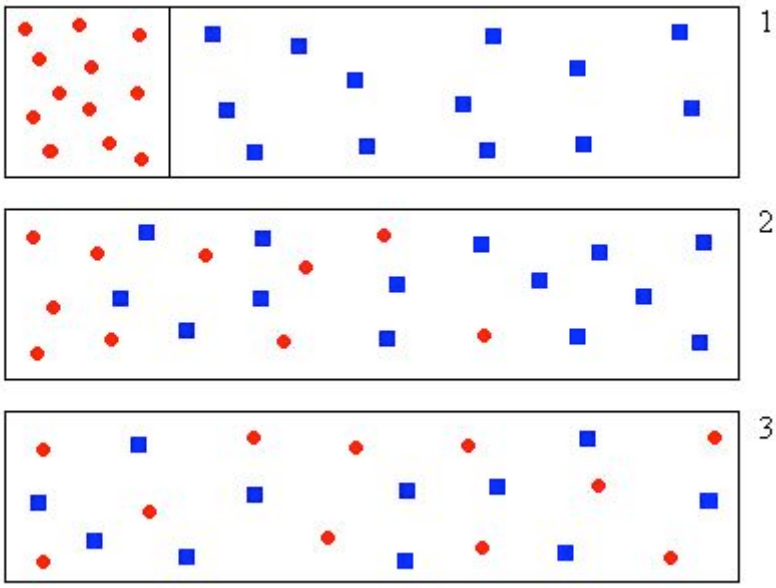

Figure 2.1 A schematic representation of the mixing of two substances by diffusion.

Comparing with gases, in liquids, the molecules are more densely packed, as so, they are more strongly affected by force fields of neighbouring molecules (they are subjected to more collisions). Cussler [2] exemplifies the difference between the diffusion rates in gaseous and liquid systems by calculating the penetration distance, which is the distance that a component diffuses through a second component. Penetration distance expressed in cm can be estimated as $\sqrt{4Dt}$, where D is the diffusion coefficient in cm^2/s and t is time in s. By considered a benzene/cyclohexane system with a diffusion coefficient of about 2×10^{-5} cm^2/s and based on the results presented in table 2.1, he was able to conclude that diffusion rates in dilute liquid systems can be thousand-fold smaller than in gases. The slow characteristic of

liquid diffusion can limit the overall rate of a process in liquid mixtures. Nevertheless, in situations where concentration gradients are large, diffusion rates can be significant [3].

Table 2.1 Penetration results for a benzene/cyclohexane gas and liquid binary system with a diffusion coefficient of 2×10^{-5} cm^2/s [3].

time, s	penetration in gases, cm	penetration in liquids, cm
1	0.3	0.004
60	4	0.03
3600	30	0.3

In a variety of chemical engineering processes, diffusion can occur simultaneously with other phenomena. Diffusion progresses at small rates, being in most of the situations, the slowest step in the sequence thus limiting the overall rate of the process. The fact that diffusion is frequently the rate limiting step of a process highlights its importance and justifies the interest of studying such phenomenon. For example, diffusion limits distillation efficiency, the rate of industrial reactions using porous catalysts, the speed at which an acid and base can react and the speed at which human intestine absorbs nutrients. It controls the growth of microorganisms producing penicillin, the rate of steel corrosion, and flavour release from food [2]. Considering the fact that diffusion has a major importance in unit operations such as distillation, extraction, absorption processes, and chemical reactions, it can be concluded that this area of study is of high importance to a chemical engineer.

It is possible to accelerate mixing processes if the solution is stirred, but the mixing still depends on random molecular motions. The stirring is not a molecular process, but a macroscopic process that moves portions of a fluid over larger distances. The macroscopic motion enables the molecular motion accelerating diffusion and mixing [2].

2.1 Fundamental laws of diffusion

This chapter issues on the historical development of the mathematical models aiming at describing diffusion phenomenon. The model description is based on fundamental laws. Two commonly used laws will be presented. A more fundamental one named Fick's law of diffusion, and a second one, which has no formal name and involves a mass transfer coefficient. Fick's law uses a diffusion coefficient and can be used to describe physical, physico-chemical, and biological processes. The other law is used implicitly in chemical kinetics and to describe medical phenomena [2].

The diffusion coefficient is more fundamental, involving the knowledge of physical properties. The mass transfer coefficients are more adequate for practical situations and rough measurements. Cussler considered the choice between the two fundamental laws as "a compromise between the ambition of obtaining a more generalised result and the available experimental resources" [2].

One of the subjects of interest of this thesis is to express our diffusion results, measured by using a novel experimental technique based on Raman spectroscopy, in the most general and fundamental way by using a diffusion coefficient model approach. The concentrations will be measured as a function of position and time and mass transfer coefficient results in a lumped parameter that involves the effects of all the mass transfer processes occurring. Here, effects of all forces, apart from the concentration gradient, e.g. friction and gravity, were eliminated. In short, mass transfer is case-specific and it is not a valid option to measure concentration as a function of position and time. Fick's law will be the applied approach.

2.1.1 Fick's law

The modern ideas of diffusion have been developed mostly by two scientists, Thomas Graham and Adolph Fick. Thomas Graham, a Scottish chemist, began his work by studying the diffusion of gases and later of liquids. His measurements are considered the first quantitative experiments on diffusion. His experiments conducted him to results that consisted of volume-change of the original gases held in the experiment. Considering the volume-change as a characteristic of diffusion Graham stated: "the diffusion or spontaneous intermixture of two gases in contact, if effected by an interchange of position of infinitely minute volumes, being, in the case of each gas, inversely proportional to the square root of the density of the gas" [2]. Thomas Graham also performed important studies on liquid diffusion, and concluded that diffusion is several thousands times slower in liquids than in gases. He also understood that diffusion has a decreasing rate along its process. Finally, he concluded that the diffusion flux is directly proportional to the concentration gradient [2].

Adolf Eugen Fick (Fig. 2.2), gave continuity to Graham's work on diffusion, and was responsible for the development of the fundamental laws of diffusion.

Figure 2.2 Adolph Fick (1829-1901) [4].

He wrote in an article published in 1855 [2]: "A few years ago, Graham published an extensive investigation on the diffusion of salts in water… It appears to me a matter of regret, however, that in such an exceedingly valuable and extensive investigation, the development of a fundamental law, for the operation of diffusion in a single element of space, was neglected, and I have therefore endeavoured to supply this omission". He introduces the basic idea of the phenomena: "The diffusion of the dissolved material… is left completely to the influence of the molecular forces basic to the same law… for the spreading of warmth in a conductor and which has already been applied with such great success to the spreading of electricity" [2]. Fick proposed an analogy using Fourier's law for heat conduction, previously applied with great success as Ohm's law for electrical conduction. Equation 2.1 shows Fick's law for mass flow rate J_1.

$$J_1 = Aj_1 = -AD\frac{\partial c_1}{\partial z} \qquad (2.1)$$

A is the area across which diffusion takes place, j_1 is the flux per unit area, c_1 is the concentration, z the distance and D is the diffusion coefficient.

Using Fourier's work, Fick also derived a more generic equation, commonly known as Fick's second law (Eq. 2.2).

$$\frac{\partial c_1}{\partial t} = D\left(\frac{\partial^2 c_1}{\partial z^2} + \frac{1}{A}\frac{\partial A}{\partial z}\frac{\partial c_1}{\partial z}\right) \qquad (2.2)$$

This equation is used for one-dimension unsteady-state diffusion when A is constant.

2.1.2 Maxwell-Stefan approach

A different approach to mass transfer is to consider the individual species in a mixture, the forces between them and, their motion. The forces can be divided into driving forces and friction forces. Maxwell-Stefan equation (Eq. 2.3) is the result of the balance between these forces [5].

$$F_1 = \sum_{2 \neq 1} \xi_{1,2} x_2 (u_1 - u_2) \qquad (2.3)$$

where F_1 if the driving force on component *1*, $\xi_{1,2}$ if the friction coefficient between the two components, x_2 is the mole fraction of component *2* and, u_1 and u_2 are the species velocities. This approach is much more general than Fick's theory. Nevertheless, for some simple but important diffusion problems, Maxwell-Stefan equation does not produce significant improvements and it may also, in other situations, lead us to totally different results [5]. Figure 2.3 illustrates the principals of Maxwell-Stefan equation.

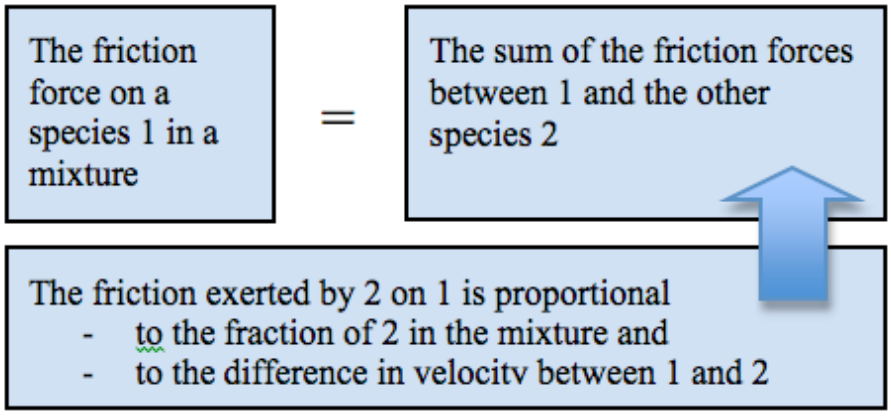

Figure 2.3 Maxwell-Stefan equation in words [5].

The diffusion driving force is the difference between components in chemical potential [5]. Chemical potential causes an internal force but external forces like gravity have also an effect in the mixture causing convection. A total potential gradient is influenced by several contributions. Equation 2.4 expresses the driving force in terms of a total gradient.

$$F_1 = -\frac{d\psi_1}{dz} \qquad (2.4)$$

where ψ_1 is total potential, result of different contributions.

For a binary liquid system at constant temperature and pressure, equation 2.4 can be rewritten into equation 2.5 where the driving force is only expressed in terms of its chemical potential [5].

$$F_1 = -\frac{d\mu_1}{dz} \qquad (2.5)$$

To avoid the mathematical complexity, it's assumed that diffusion can only occur in one direction and consider the flow near the interfaces ("film" model) [5]. Equation 2.6 shows the difference form of the driving force for a given temperature and pressure.

From the chemical potential gradient we can derivate a new form of the driving force in terms of the species activities [5]. Equation 2.6 also shows this derivation

$$F_1 = -\frac{\Delta\mu_1}{\Delta z} = -RT\frac{\Delta \ln a_i}{\Delta z} \approx -\frac{RT}{a_1}\frac{\Delta a_1}{\Delta z} \qquad (2.6)$$

where μ_1 is the chemical potential and a_1 the activity of component *1* activity. These activities are calculated using activity coefficients. Equation 2.7 shows the calculation of these activities.

$$a_1 = \gamma_1 x_1 \qquad (2.7)$$

where γ_1 is the activity coefficient and x_1 the molar fraction of component *1*.

It's also possible to relate the friction coefficient and the Maxwell-Stefan diffusion coefficient. This relation is presented in equation 2.8.

$$Đ_{1,2} = \frac{RT}{\zeta_{1,2}} \qquad (2.8)$$

$$-\frac{d\left(\ln\left(\gamma_1 x_1\right)\right)}{dz} Đ_{1,2} = x_2\left(u_1 - u_2\right) \qquad (2.9)$$

Equation 2.3 can be rewritten in a most practical form. Using equations 2.6, 2.7, and 2.8 we obtain equation 2.9, a new form of Maxwell-Stefan equation.

2.2 Diffusion coefficients

The Fick diffusion coefficient is a factor of proportionality that represents the amount of substance diffusing across a unit area through a unit concentration gradient in a unit time. In the chapter 2.1 the diffusion coefficient was treated as proportionality constant. From equation 2.1, Fick law, the diffusion flux is proportional to its concentration gradient in function of time and proportional to a constant *D* defined as Fick's diffusion coefficient. Maxwell-Stefan equation describes diffusion fluxes in terms of gradients in activities and Maxwell-Stefan diffusion coefficient. The diffusivities can be transformed into one another. The relation between both diffusion coefficients is

$$D = \Gamma Đ \qquad (2.7)$$

where *Đ* is the Maxwell-Stefan diffusion coefficient and *D* the Fick diffusion coefficient. Γ is a thermodynamic correction factor defined by equation 2.8.

$$\Gamma = 1 + x_1 \frac{\partial \ln \gamma_1}{\partial x_1}\bigg|_{x_2,T,P} \qquad (2.8)$$

Maxwel-Stefan theory separates thermodynamics and mass-transfer, while Fick's theory assumes both effects in one coefficient, illustrated in equation 2.7. This fact makes Maxwell-Stefan theory advantageous for modelling, as it is less concentration dependent [1].

2.3 Determination of diffusion coefficients

Diffusion has been gaining the importance that other properties like vapour-liquid equilibria or viscosities had. Diffusion coefficients can be obtained either experimentally or using empirical correlations. The development of new technology and sophisticated models is contributing to an improvement in the accuracy of diffusion coefficients prediction [1].

2.3.1 Experimental methods for determining diffusivities

This chapter gives an insight into the experimental measurement of diffusion coefficients in liquids. Experimental methods are needed, as they provide more accurate results than empirical correlations, even at higher concentrations. Several physical and chemical experimental methods can be applied [6] and a survey of different techniques for diffusion coefficients measurement is detailed described by Wakeham [7].

The measurement of diffusion coefficients in liquids is a very slow process and one experimental determination can last several days. This measurement time constraint is the reason why experimental results are scarce in literature [7]. On the other hand, some powerful techniques have been developed for the measurement of diffusion coefficients, such as the ones based on interferometric methods to NMR measurements and chromatographic flow-broadening [7], thus improving the success of achieving reliable experimental data. Wakeman suggests the work of Millat [8] for further reading about these methods.

Some of the methods used to measure diffusivity coefficients are based on the optical interferometer technique. Optical techniques became more accurate and efficient with the application of laser power light sources. Between several optical techniques, the holographic interferometric technique is the most widely used [6]. The scarcity of its industrial application is related to the rigorous optical conditions required. Consequently other simpler techniques have a wider industrial application, one example being the multiple beam interferometer, which, on the other hand, presents limitations related with the acquisition of

extreme points in the interferogram. Chhaniwal suggests Anand's work [9] for further information on this technique. For transparent liquids, Michelson interferometer technique is reported by Chhaniwal as a suitable technique to be used for diffusion coefficients determinations purposes [6].

According to Bosse, in the last decades the holographic interferometry and the Taylor dispersion were the most used techniques being the Taylor dispersion the choice for diffusion coefficients measurements in diluted binary systems [1]. Both techniques qualitatively predict similar results but the Taylor dispersion method is the less experimental demanding. All diffusion coefficients measurements, in concentrated or diluted solutions, can be predicted by using the standard HPLC-equipment. Bosse suggests the work of Ven-Lucassen [10] for further reading regarding diffusion coefficients measurement using HPLC [1].

For multicomponent systems the use of holographic interferometry, instead of Taylor dispersion, is recommended [1]. In this case, Taylor dispersion experimental setup and the corresponding data processing, is more laborious and the results less accurate.

In conclusion, no matter the used technique, the measurement of diffusion coefficients in binary systems requires a high experimental effort and very time-consuming data processing steps. Consequently, the reduction of experimental effort for diffusion measurements is one of the goals of this work, and an optical technique called Raman spectroscopy, will be tested for that purpose. The principles of Raman technique will be presented and discussed in a latter section.

2.3.2 Prediction of diffusion coefficients

This chapter gives the fundamentals needed to predict diffusion coefficients in liquids being noteworthy that no general theory is able to predict, *a priori*, an accurate value for the available diffusion coefficients [2]. Its prediction is largely dependent on experimental results and experimental measurements are considered difficult [2].

State theories used for diffusion coefficient prediction are quite idealized. The theories are not reasonable for calculating diffusion coefficients but they provided the frame for valuable prediction methods [3].

The Stokes-Einstein equation (equation 2.11), which strictly applies only to macroscopic systems, is used as frame in developing correlations for molecular diffusion. It is the most commonly used method for estimating diffusion coefficients in liquids but, the accuracy of the estimated coefficients is only around twenty percent [11].

$$D = \frac{k_B T}{f} = \frac{k_B T}{6\pi\mu R_0} \qquad (2.11)$$

f represents the friction coefficient of the solute, k_B is the Boltzmann´s constant, μ is the solvent viscosity, and the R_0 is the solute radius. Solvent viscosity and solute radius are two important variables that may influence significantly the diffusion coefficient prediction. On the contrary, the temperature variation does not cause large effects. [2]

Molecular motion in a liquid takes place at high density (Fig. 2.4). As a consequence, it involves many interactions and vacancies making the kinetics associated to this motion quite complex. Stokes-Einstein equation uses a simplified model, derived assuming a rigid solute sphere diffusing in a continuum solvent, as described schematically in figure 2.4.

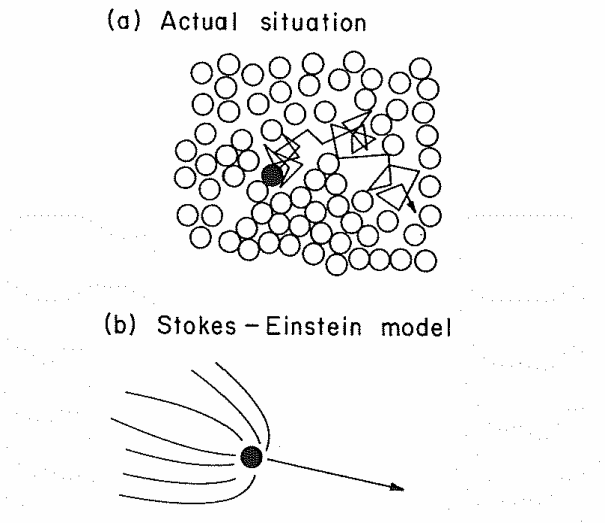

Figure 2.4 Molecular motions in a liquid. (a) Molecular motion in a liquid. (b) Model of a solute sphere in a solvent continuum [2].

For liquid mixtures at infinite dilution, this assumption works well but if the solute size is five times smaller than the solvent, equation 2.11 fails [12]. The smaller the solute size is the bigger is the error. In high-viscosity solvents prediction error is very high. However, for a high viscosity medium, diffusion may become independent of viscosity [2].

Different correlations were developed in order to overcome the limitations of Stokes-Einstein equation. These correlations were developed for cases in which the solute and the solvent have similar sizes. All these correlations, similarly to Stokes-Einstein equation, are temperature and viscosity dependent [3].

A binary system of solute *1* in solvent *2* at infinite dilution means that *1* is diffusing in an infinitely dilute solution of *1* in *2*, implying that every molecule of *1* is in pure *2*. This assumption is true and the diffusion coefficient is representative up to concentrations of 5 to 10 mol-% [3]. Next, the correlations methods are presented. These methods are useful to estimate the diffusion coefficient at infinite dilutions. The first method presented is Scheibel correlation:

$$D_{12}^{\circ} = \frac{A\,T}{\eta_2 (V_1)^{\frac{1}{3}}}\left[1+\left(\frac{3V_2}{V_1}\right)^{\frac{2}{3}}\right] \qquad (2.12)$$

where D_{12}^{0}, in cm^2/s, is the mutual diffusion coefficient of solute *1* in solvent *2*. The solute *1* concentration is very low. V_1 *and* V_2, in cm^3/mol, is the molar volume of solute and solvent, respectively, T, in K, is the temperature and η_2, in cP the solvent viscosity. Constant A is equal to 8.2×10^{-8}, except as follows: 25.2×10^{-8} for water if $V_1<V_2$, 18.9×10^{-8} for benzene when $V_1 < 2\times V_2$, and 17.5×10^{-8} for others if $V_1 < 2.5\times V_2$ [3].

Wilke-Chang [3] (Eq. 2.13), is a commonly used correlation for predicting diffusion coefficients at infinite dilution. It is an empiric modification of Stokes-Einstein equation (Eq. 2.11) where the concentration of solute *1* is very low.

$$D_{12}^{0} = \frac{7.4\times10^{-8}(\phi\, M_2)^{1/2} T}{\eta_2 V_1^{0.6}} \qquad (2.13)$$

M_2, in g/mol, is the solvent molecular weight, V_1, in cm^3/mol, is the molar volume, T, in K, is the temperature and η_2, in cP, the solvent viscosity. If the solvent is water, ϕ is recommended to be 2.6. If the solvent is methanol, 1.9, 1.5 if it is ethanol, and 1 if it is unassociated. Tyn and Calus proposed a different type of method:

$$D_{12}^{o} = 8.93\times10^{-8}\left(\frac{V_1}{V_2^2}\right)^{1/6}\left(\frac{P_2}{P_1}\right)^{0.6}\frac{T}{\eta_2} \qquad (2.14)$$

where solute *1* concentration is very low. V_1 *and* V_2, in cm^3/mol, are the molar volumes of the solute and the solvent, respectively, T, in K, is the temperature and η_2, in cP, the solvent viscosity. P_1 *and* P_2 are the solute and solvent parachors. The parachors are related with the liquid surface tension, as can be seen from equation 2.15.

$$P = V\,\sigma^{1/4} \qquad (2.15)$$

σ, in dyn/cm, is the surface tension and V, in cm^3/mol, is the molar volume. Both parameters measured at the same temperature. P is tabulated for a large number of components [13], but it can be also predicted from addictive group contributions [3].

When predicting mutual diffusion coefficients at infinite dilution, the Tyn and Calus method produce quite acceptable results, normally with an error less than 10 %. However, the parachors of both the solute and the solvent should be known. This limitation originated the development of a modified Tyn-Calus equation (Eq. 2.16).

$$D_{12}^{o} = 8.93\times10^{-8}\,\frac{V_2^{0.267}}{V_1^{0.433}}\,\frac{T}{\eta_2}\left(\frac{\sigma_2}{\sigma_1}\right)^{0.15} \qquad (2.16)$$

Hayduk and Minhas proposed different correlations for the different infinite dilution binary diffusion coefficient depending on the type of solute-solvent system [3]. Hayduk-Minhas correlations for normal paraffin mixtures, for solutes in aqueous mixtures or non-aqueous mixtures are presented in [3]. Equation 2.17 is Hayduk-Minhas correlation for non-aqueous infinite dilution binary systems.

$$D_{12}^{o} = 1.55 \times 10^{-8} \frac{T^{1.29}}{\eta_2^{0.92} V_2^{0.23}} \frac{P_2^{0.5}}{P_1^{0.42}} \qquad (2.17)$$

The terms are the same as described in Tyn-Calus equation (Eq. 2.14). In fact, both equations are similar and the same restrictions apply for both methods. If we eliminate the parachors, the obtained mathematical expression results on the modified Hayduk-Minhas equation (Eq. 2.18).

$$D_{12}^{o} = 1.55 \times 10^{-8} \frac{V_2^{0.27}}{V_1^{0.42}} \frac{T^{1.29}}{\eta_2^{0.92}} \frac{\sigma_2^{0.125}}{\sigma_1^{0.105}} \qquad (2.18)$$

Considering that the diffusion coefficient in liquids varies with the solute concentration, it can be concluded that the Stokes-Einstein equation or its empirical extensions are limited to infinitely dilute solutions [2]. The concentration dependence of binary coefficients is complicated. It might vary linearly between two limiting diffusion coefficients or not. The diffusion coefficient D_{12} in a binary system may be proportional to a thermodynamic factor, a as expressed in equation 2.19 [3].

$$\alpha = \left[\frac{\partial \ln a_1}{\partial \ln x_1} \right]_{T,P} \qquad (2.19)$$

The Darken equation (Eq. 2.20) relates D_{12} to composition. Initially used for studying diffusion in metals, it was further extended to organic liquid mixtures. It works well for mixtures which components may solvate [3].

$$D_{12} = \left(D_1^* \, x_1 + D_2^* \, x_2 \right) \alpha \qquad (2.20)$$

Due to the unavailability of tracer diffusion coefficients D_1^* and D_2^*, equation 2.20 was rewritten as equation 2.21.

$$D_{12} = \left[x_1 \left(D^{\circ}_{21} - D^{\circ}_{12} \right) + D^{\circ}_{12} \right] \alpha \qquad (2.21)$$

Equation 2.21 is simpler to use because diffusion coefficients at infinite dilution, D°_{21} and D°_{12}, are easier to estimate by a variety of different methods, as described above. One should note that D_{12} is a linear function of composition that is corrected by thermodynamic

factor, a. Plotting a and D_{12} as a function of x_1, the obtained traces have similar curvature, which validates the use of a as a correction factor [3].

Another suggestion is that $D^{12}\times\eta\times a^{-1}$ should be a linear function of the molar fraction. Nevertheless, Vignes proved that it was not valid for the systems acetone-water and acetone-chloroform. Later, according to Rao and Bennett, for different non-ideal mixtures, $D^{12}\times\eta\times a^{-1}$ doesn't vary substantially with the composition and no explicit linearity in function of composition was discerned. In addition to this theory, Carman and Stein stated that $D^{12}\times\eta\times a^{-1}$ is only a linear function of the composition for the nearly ideal system benzene-carbon and for the non-ideal system acetone-chloroform [3].

A new convenient way to correlate the composition effect was suggested by Vignes that proposed a geometric average (Eq. 2.22) instead of arithmetic one [3].

$$D_{12} = \left[\left(D_{12}^{\circ}\right)^{x_2} \times \left(D_{21}^{\circ}\right)^{x_1}\right]\alpha \qquad (2.22)$$

Equation 2.22 proved to deliver good agreements with experimental data. According to [3], Dullien's study shows that Vignes correlation fits experimental data for ideal or nearly ideal systems but for nonideal systems the correlation doesn't produce very accurate results. Although, Dullien proved that Vignes' proposition slightly improved accuracy, Tyn and Calus showed that the deviation for the Vignes correlation for ethanol-water, acetone-water and acetone-chloroform systems was approximately 14%.

The thermodynamic factor a has to be known. For Non-Random Two Liquid model (NRTL) (Eq. 2.23) and Wilson (Eq. 2.24) equations, a is given by equation 2.25.

$$\frac{G_m^E}{RT} = x_1 x_2\left(\frac{\tau_{21}\, G_{21}}{x_1 + x_2\, G_{21}} + \frac{\tau_{12}\, G_{12}}{x_2 + x_1 G_{12}}\right) \qquad (2.23)$$

$$\frac{G_m^E}{RT} = -x_1 \ln\left(x_1 + \Lambda_{12}\, x_2\right) - x_2 \ln\left(x_2 + \Lambda_{21}\, x_1\right) \qquad (2.24)$$

$$\alpha = 1 - 2\frac{G_m^E}{RT} \qquad (2.25)$$

R is the gas constant, T the temperature, a is the thermodynamic factor and x_1, and x_2 are the molar fraction of component *1* and *2*, respectively. G_m^E, Λ, G, and τ are the parameters of NRTL and Wilson equations.

No correlation method is always satisfactory [2]. The Vignes method (Eq. 2.22) has been, however, intensively tested and proven to provide accurate results for a considerable number of different systems. It is simple and independent from viscosities [3]. In the experimental

section of this thesis, diffusivities were predicted using Vignes method and compared with the obtained experimental results. A discussion on this matter is presented in chapter 3.

2.4 Multicomponent diffusion

In the previous chapter, it was considered that diffusion takes place in binary systems, i.e. systems containing only one solvent and one solute. The presented systems were dilute solutions, in which the solute is present at low concentrations in a pure solvent. It was shown that the diluted systems could be analysed much more easily than the concentrated ones. The concentration dependence of diffusion coefficients is considered complicated [2]. This section describes diffusion in multicomponent systems.

Apart from binary systems, other diffusion processes where the transport of many solutes takes place in nature. Many processes, for example physiological processes, involve simultaneous diffusion of many different solutes. One well known physiological process occurring in the blood is the diffusion of oxygen, sugars and proteins.

According to Cussler, the description of multicomponent diffusion is of limited value. Firstly, the majority of solutions are diluted, and the multicomponent effect in dilute systems is minor. Secondly, some multicomponent effects are often better described when the complex equations that describe multicomponent diffusion are not used. Even so, some concentrated systems can be better described using multicomponent diffusion equations, i.e., systems that involve unusual chemical interactions like solutes of very different sizes, solutes in highly nonideal solutions, concentrated electrolytes, or concentrated alloys [2].

The equations used in the description of multicomponent diffusion can be empirical generalizations of Fick's law. For an *n*-component system, the equation has $(n-1)^2$ diffusion coefficients implying that one of the components has to be designated as the solvent. The coefficients have to obey to certain restrictions, and not all are independent. These constraints reduce the number of diffusion coefficients required to describe diffusion for an n-component system. However, the application of these restrictions requires detailed thermodynamics information that is not often available. As a result, the system is often treated as having $(n-1)^2$ independent diffusion coefficients.

Maxwell-Stefan equation is an alternative to the generalisation of Fick's equation. This approach has two main advantages: firstly, the diffusion coefficients are the binary values found from binary experiments or calculated using the Chapman-Enskog theory, and secondly, Maxwell-Stefan equation does not require the definition of one component as solvent. On the other hand, Maxwell-Stefan approach also has some disadvantages. It is most often adequate to dilute gases, and if used with liquids diffusion coefficients cannot be the ones from for the

binary systems. Moreover, it is complex to combine with mass balances without designating one component as solvent. After presenting the pros and cons of Maxwell-Stefan approach, Cussler stated: "…both advantages of this form are often lost" [2].

The origins of the generalised Fick's equation for multicomponent diffusion can be analysed using irreversible thermodynamics. According to Cussler, "irreversible thermodynamics does give the proper form of the flux equations and clarifies the number of truly independent coefficients" but he considered this information pointless as it may be obtained experimentally. About the nature and magnitude of the coefficients in the multicomponent equations nothing can be concluded from irreversible thermodynamics, as pointed out by Cussler "irreversible thermodynamics has enjoyed an overoptimistic vogue…is of limited utility in describing multicomponent diffusion" [2].

3 Raman spectroscopy and its application in diffusion studies

Raman and infrared (IR) spectroscopy are defined as vibrational spectroscopic techniques, i.e. they are based on molecular vibrations. Based on the characteristic spectral patterns, these techniques allow the identification and quantification of different substances in samples of different physical states with minor or no sample pre-preparation and without destroying it [14]. Infrared absorption is still the most widely used of these two complementary techniques, but the application of Raman spectroscopy is growing rapidly. The main advantages of Raman spectroscopy (in comparison with IR) are the easiness of *in situ* analysis and its feasibility to analyze aqueous solutions [15].

Raman spectroscopy was named after C.V. Raman (1888-1970) that together with K.S. Krishnan has, for the first time, experimentally observed the phenomenon of inelastic scattering of light in 1928. This phenomenon was previously postulated by A. Smekal (1895-1959) in 1923 [16]. Professor C.V. Raman focused sunlight onto a sample by using a telescope. Then, he placed a second lens between the sample and the optics filters to shown the existence of scattered light radiating at different frequency from the incident light. Due to this work he was awarded with the Nobel Prize in Physics in 1930 [17]. Despite the long history, Raman spectroscopy development has been slow and its applications limited until the 1990's when the technological advances in instrumentation contributed to minimize the common difficulties associated with sample degradation and fluorescence [15].

A detailed explanation regarding the Raman effect is given in chapter 3.1. In chapter 3.2, the instruments that compose the Raman spectroscopy technique are presented. A summary about the recent scientific works that use Raman spectroscopy as mean of study of diffusion in liquids is given in 3.3.

3.1 The principles of Raman spectroscopy

When an incident monochromatic light interacts with a sample, the photons, which make up the light, can be absorbed, scattered or may not interact with the material thus being transmitted through it. When the energy of the incident light corresponds to the energy gap between the ground state of a molecule and its excited state, the light is absorbed, the molecule is promoted to a higher energetic excited state and then, the light may be emitted. The absorption and emission phenomena are the basis of several spectroscopic

techniques, for example acoustic spectroscopy, X-ray, NMR, EPR, electronic absorption, fluorescence emission, vacuum ultraviolet, and infrared absorption.

Light scattering occurs when the incident photon of energy does not match the molecule energy gap between the ground state and its excited state. The scattered light can be collected at a certain angle relative to the incident light beam, assuring that there is no absorbed light, which has similar energy to that of the incident light. Raman technique is the most used scattering technique for identification purposes, but the scattering phenomenon is also exploited in techniques for measuring particle size and size distribution down to 1μm sizes.

Incident light, employed in infrared and Raman spectroscopy, has different characteristics. In infrared spectroscopy, radiation covering a range of frequencies is employed, and when a frequency of the incident radiation matches the vibrational energy of the molecule it promotes it to an excited state. The radiation at that frequency is then absorbed, and thus it will not be detected in the beam after passing through the sample. In Raman spectroscopy the incident light radiates at one single frequency and the detector measures the scattered radiation from the molecule, one vibrational unit of energy different from the incident light. The incident photons polarize the electronic cloud of the molecule promoting the formation of a short time state, commonly defined as “virtual state” that quickly loses its stability and re-radiates the photon.

When the incident radiation causes only an electron cloud distortion, the photons are scattered with very small frequency changes. This scattering process is elastic, and for molecules it is defined as Rayleigh scattering (Fig. 3.1).

If the incident radiation is able to promote nuclear motion, energy is exchanged between the incident photons and the molecule causing an inelastic phenomenon. In an inelastic phenomenon the scattered photons energy is different from that of the incident photon. This is the Raman scattering (Fig. 3.1).

In summary, the light scattered from a molecule can be described as (1) Rayleigh scattering and (2) Raman scattering (Fig. 3.1). The latter can be divided into Stokes (if the scattered photon has lower energy than the incident photon) and Anti-Stokes (if the scattered photon has higher energy than the incident photon). The intensity of the Stokes scattering is much higher than Anti-Stokes scattering, thus it is highly preferred in conventional Raman spectroscopy [15].

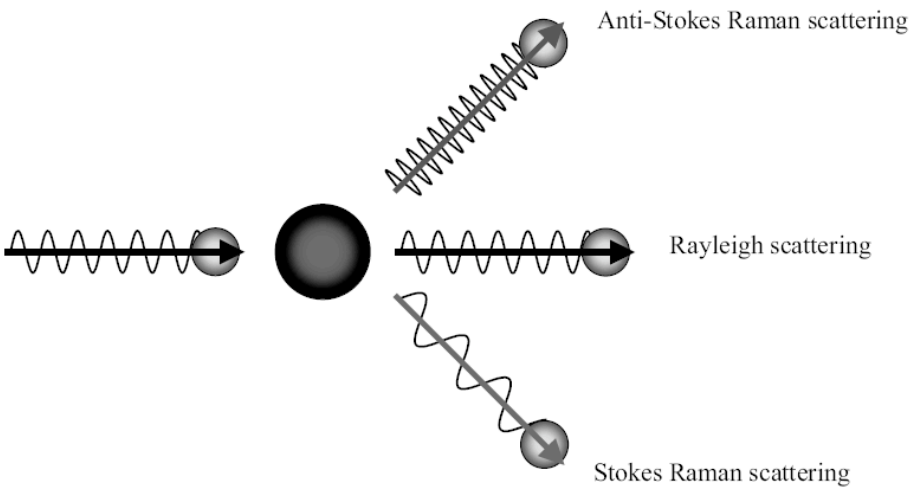

Figure 3.1 Rayleigh and Raman scattering. [15]

Another phenomenon that may occur simultaneously with Raman scattering is fluorescence. Raman scattering and fluorescence are in fact two competitive phenomena. Fluorescence is an optical phenomenon, in which the molecular absorption of a photon causes the emission of a photon with higher wavelength, i.e. with lower energy. If fluorescence is generated, it is often more intense than Raman scattering, and thus it can completely obscure the Raman signal. For a better understanding, figure 3.2 presents a diagram with the mechanisms of Rayleigh and Raman scattering and fluorescence emission.

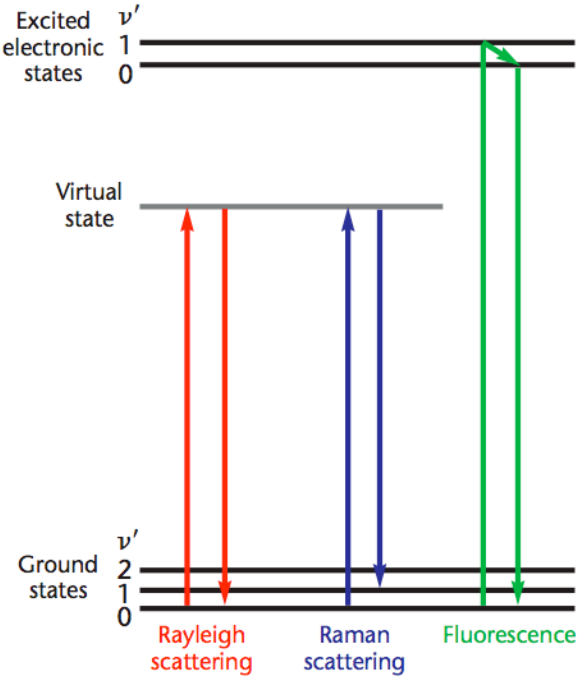

Figure 3.2 Mechanisms of various light scattering processes [14].

Raman effect is considered a weak phenomenon because only one photon in around 10^8 photons is inelastically scattered. To increase the intensity of Raman scattering, a high

beam source should be applied. High power densities are usually delivered to small samples using modern lasers in order to obtain sufficient scattering intensity.

A straightforward choice for obtaining a higher scattering intensity is to increase laser power. However, the use of a high laser power or a higher frequency, for example the UV region, may degrade the samples. Visible laser or near infrared laser are usually preferred for the excitation, nevertheless for visible excitation fluorescence of the samples may occur [14].

3.2 Raman instrumentation

The laser sources became more widely available in 1970s causing a revolution in Raman spectroscopy [15]. Before the introduction of lasers as the excitation sources, spectral accumulation times were typically measured in hours so it was simply not practical to use Raman scattering [15]. Modern lasers join to favorable factors, higher power intensity and the use of low wavelength, making the technique sensitive enough to analyze small samples. The occurrence of sample degradation and fluorescence are the main problems encountered in modern Raman spectroscopy.

Raman instruments built before 1990 used a configuration with multiple stages to differentiate the much more intense elastically scattered light from the Raman scattered light. In the 1990s, it was recognized that holography could produce a notch filter that, basically, would block the entire laser light but allowing the Raman light to pass [18]. Nowadays, in general, all instruments use monochromatic laser sources with wavelengths comprised between 200 nm and 1.06 μm. The obtained spectrum should be independent of the used excitation wavelength; nevertheless, resonance phenomena could appear and may affect the scattering pattern. In conclusion, considerations such as the optimization of the signal intensity or avoidance of fluorescence interference dictate the selection of a particular laser wavelength source. This issue is of particular importance and crucial for Raman spectroscopy implementation [18].

The most widely used Raman spectrometers are of dispersive or Fourier Transform (FT) type. Basically, a Raman instrument consists of an excitation source (laser source), a sample illumination system, a wavelength selector, and a detector. Figure 3.3 presents a simplified scheme of a Raman spectrometer putting in evidence its components. The dispersive instrumentation incorporates a monochromator grating with a multichannel charge-coupled device (CCD) detector [18]. It filters the collected scattered light rejecting all the light at the incident laser frequency. It collects the scattering light using a sampling angle of 90º or 180º degrees. Another method to collect the scattering light consists of using fiber optic. Fiber optic methods are coming more popular due to their easy use and remote sensing

capability [19]. Before the spectrum registration, the detector discards the undesirable wavelengths. FT Raman instrumentation uses a Michelson interferometer and extracts the spectrum by performing a Fourier transform of the generated interferogram [18].

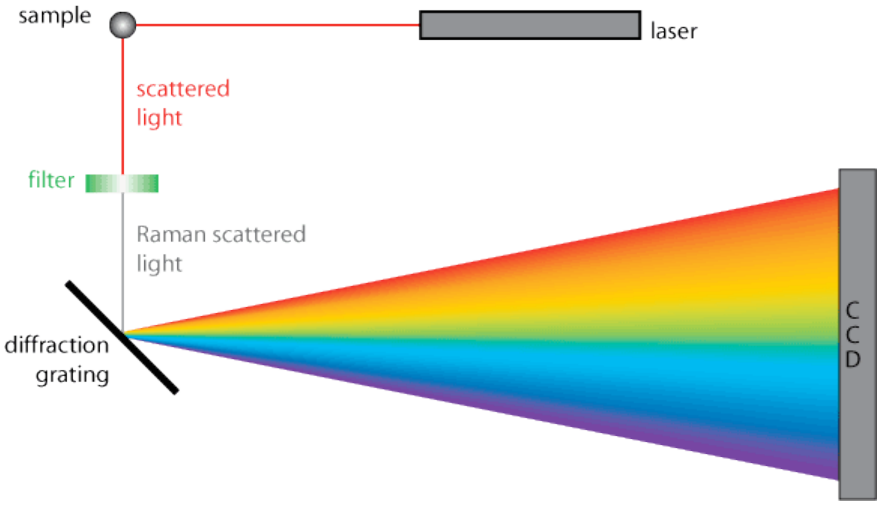

Figure 3.3 Simplified diagram of Raman spectrometer's operation [20].

The introduction of optical fibers has significantly contributed to the application of Raman spectroscopy both in field measurements (portable equipments) and process monitoring (online measurements). The optical fibers are used to transmit the laser light, collect and transmit the spectral signal to the detector over distances that can reach a few hundred meters [18]. Since problems may arise as the length of the probe increase, especially in the case of highly scattering samples, filtered Raman probes are required to minimize problems with silica Raman background signals [21].

Microprobes enhanced the rejection of fluorescence and made the system easier to operate. Moreover, they have also opened the opportunity for Raman microscopy analysis taking advantage of high spatial resolution (better than 1 μm) [22].

Raman microscopy is a technique that can tightly focus a sample using a microscope objective and allows the Raman light to be collected and transferred to a spectrometer. It detects the spectra of molecules absorbed on surfaces and enables the selection of the measurement points avoiding sample inhomogeneities. It enables the study of minute sample quantities, multilayer and heterogeneous samples. Micro-Raman opened the way for Raman imaging applications. Raman microscopy can offer a powerful non-destructive and non-contact method of sample analysis.

The extraction of information related to chemical changes, dilutions and physical mixing from Raman spectra become simpler with the implementation of remote, fiber-based sampling systems that allow chemical or physical processes to be followed *in situ*.

3.3 Diffusion measurements in liquids by Raman spectroscopy

Measuring diffusion coefficients trustworthy and reliably is reputed to be difficult, and only few systems have been studied. The available data on diffusion coefficients, even for binary mixtures, is scarce. The established diffusion measurements are laborious, time consuming and requires specialized equipment. A significant number of experiments are needed to predict multicomponent diffusion coefficients at a single composition. In such context, Raman is a viable methodology since it can overcome some of the typical drawbacks of the conventional methods.

Typically, the methods used to measure diffusion in binary and multicomponent are: interferometry [23] and Taylor dispersion [24]. However, these two methods imply long experiments and are disadvantageous when applied to multicomponent systems [25]. Bardow (one of the pioneers of Raman methodology) considered that "The main drawback of these methods is that they rely on scalar quantities like refractive index or the conductivity, which cannot be associated unambiguously with concentration in the case of multicomponent systems" [25].

Techniques based on spectroscopy allow direct determination of the molar fractions of all components in a mixture. Moreover, they allow fast measurements. Having this advantage in consideration, Bardow's research group has developed new procedures for the measurement of diffusion in liquids using Raman spectroscopy and model-based techniques for the analysis and design of the experiments [25]. Fick's diffusion coefficients are strongly dependent from composition [26]. Using Raman spectroscopy, this dependence can be predictable from experimental points that are then interpolated using a low-order polynomial function [25].

Bardow and co-workers have successfully used Raman spectroscopy for diffusion measurements in binary and ternary liquid mixtures [26, 28 and 29]. They have optimized the method improving spatial and temporal high-resolution. Concentration profiles with satisfactory accuracy and resolution for the prediction of diffusion coefficients were obtained. The developed methodology provided a considerable reduction of experimental work since the model-based method proposed allows predicting the concentration dependence of diffusivity using a single measurement [25]. The methodology was validated using the binary systems toluene+cyclohexane [25] and ethyl acetate+cyclohexane [28], and a ternary system n-propanol+1-chlorobutane+n-heptane [27].

Raman technique was also applied by Berg *et al*. to determine diffusion coefficients in binary liquid mixtures [16]. The research group of Berg performed two kinds of diffusion measurements in three binary liquid systems. Firstly, diffusion across the interface between

pure benzene and n-hexane was studied. Secondly, diffusion study was performed in solutions of benzene and cyclohexane or acetone with different composition. Berg reported that the predicted diffusion coefficients for benzene+cyclohexane were much lower when compared with literature values [16]. The best fit came out with a diffusion coefficient of 1.11×10^{-5} cm^2/s at an average benzene composition of 0.47. For the system benzene+acetone, however, a good agreement with the literature was found [16]. Figures 3.4 and 3.5 reported the comparison between Berg research group results and literature data, respectively for benzene+cyclohexane and benzene+acetone systems.

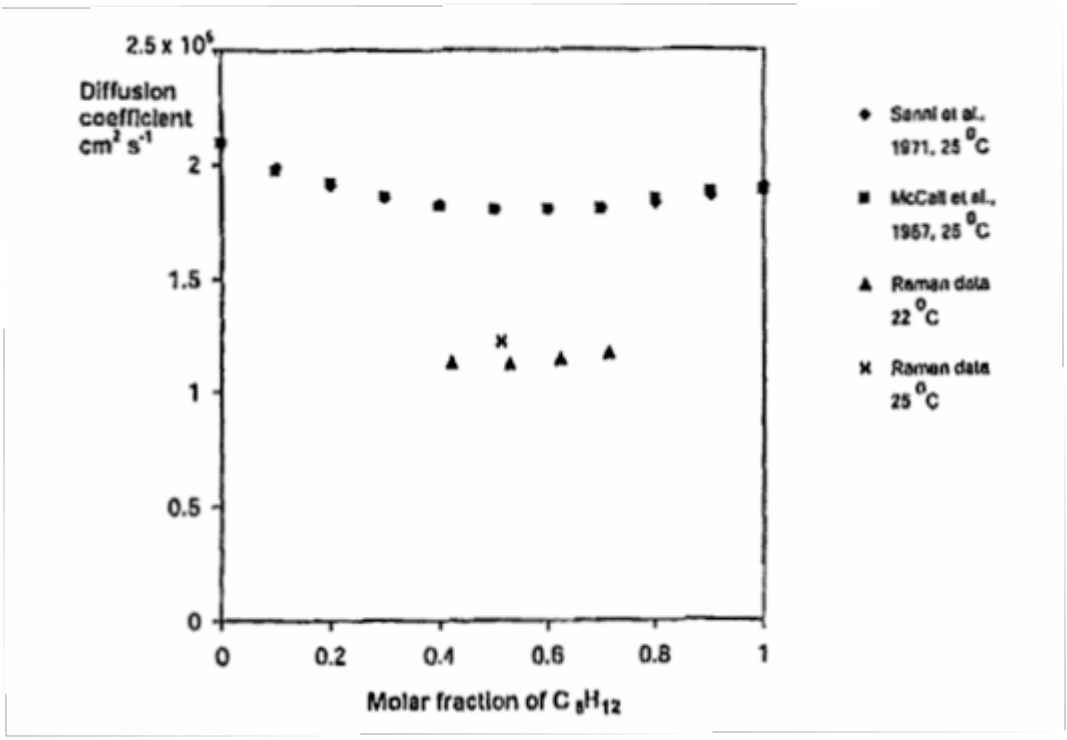

Figure 3.4 Comparison between the experimental results of Berg et al. and literature data for benzene + cyclohexane system [16].

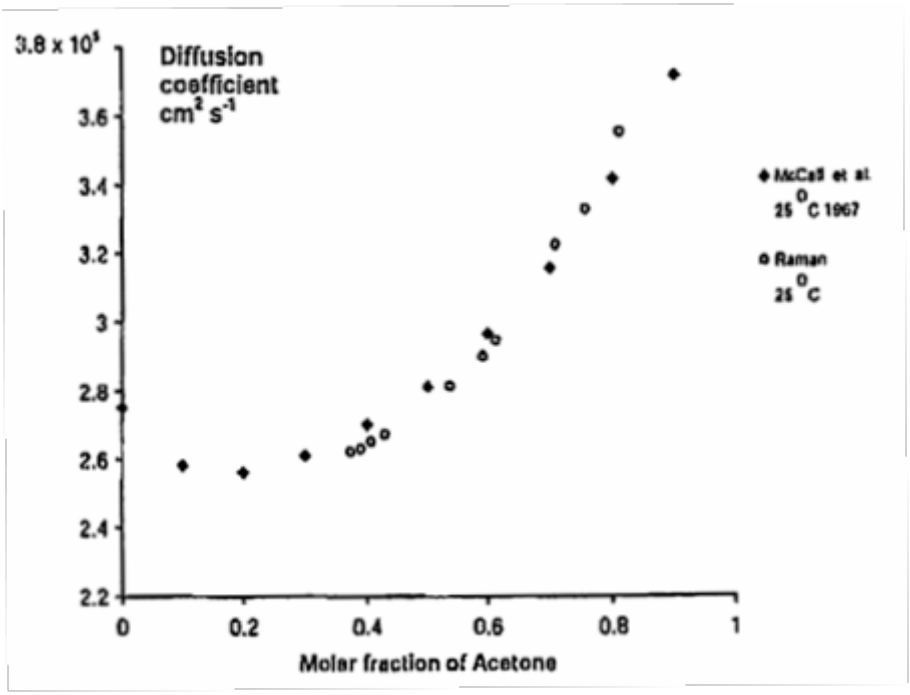

Figure 3.5 Comparison between the experimental results of Berg et al. and literature data for benzene + acetone system [16].

In these, studies diffusion occurs in a thermostated cell that enables vertical (exchange) diffusion. Direct and precise predictions of the molar fractions in the mixtures were determined by Raman spectroscopy.

Berg's work was supported by five assumptions: (1) the spectra of the substances has to be discernible enough, (2) diffusion front should not reach the upper or the lower boundaries during the measurements, i.e. the diffusion cell should be high enough, (3) it should be possible to create a boundary between the mixtures at the beginning of the experiment, (4) the interphase between the mixtures should not move during the measurements, and (5) diffusivities must be constant versus the concentration.

To analyse the spectra, both Bardow's and Berg's methodologies used curve-fitting approaches. Berg also reported that Lorentzian peak shapes gave more reliable results [16]. Figure 3.6 shows an example of the peak-fitting operation. The areas of under the characteristic peaks were chosen for quantification. It is relevant to mention that the characteristic peaks of the components should be chosen carefully, in such a way that they do not overlap.

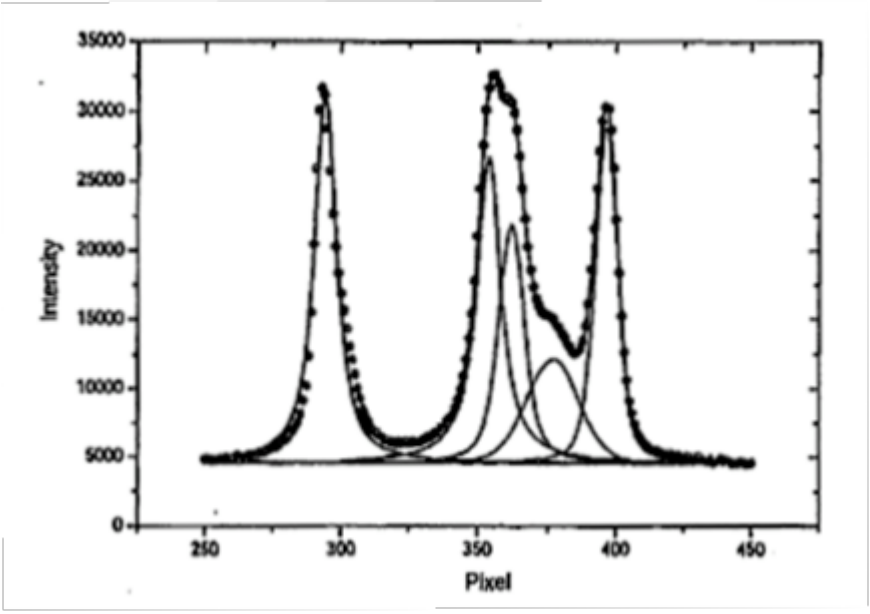

Figure 3.6 Raman spectrum of benzene+cyclohexane mixture of known concentration and the corresponding peak-fitting operation result [16].

Summarizing, Bardow's and Berg's research groups can be considered as the former groups in what concerns the development of model-based Raman spectroscopy methodologies to perform diffusion studies. Bardow's approach (in fact the pioneer work) is considered to be very thorough and robust. Comparatively, Berg's methodology is mentioned as providing highly reproducible results using a less cumbersome and a less time and consuming methodology.

4 Diffusion studies in liquids by Raman spectroscopy

This chapter describes the experimental setup and methodology used to perform the diffusion studies by Raman spectroscopy. The generally used procedure can be divided into three main steps: (1) acquiring the Raman spectra of pure components in order to identify the characteristic peaks to be used in data treatment, (2) acquiring the Raman spectra of solutions with different concentrations in order to perform calibration, and (3) performing the diffusion experiment. The third point requires cell filling with two solutions of different composition (upper and lower solutions touching at a sharp interface) to create a concentration gradient.

In the beginning of the chapter, the model compounds selected are introduced. The mathematical data treatment and the diffusion models utilized are then presented. In the end of the chapter, the predictive methods used in comparison are presented.

4.1 Chemicals

Ethanol (EtOH) and ethyl acetate (EtOAc) are used as model compounds in the present study. A summary of the relevant properties of these two solvents are listed in table 4.1. Ethanol (ETAX Aa 99.5 % purchased from Altia) and ethyl acetate (analytical grade, purchased from Merck), were used directly without further purification to acquire the corresponding Raman spectra and to prepare the solutions for the calibration and for the diffusion assays.

Table 4.1 Solvents' properties: molecular weight (M), specific gravity (ρ), molar volume (V), viscosity (η), and surface tension (σ) [30].

	M, g/mol	ρ, g/cm^3	V, cm^3/mol	η, cP	σ, dyn/cm
Ethanol	46.070	0.794	58.680	1.263	21.990
Ethyl acetate	88.120	0.895	98.560	0.426	23.750

Figure 4.1 presents the Raman spectra of ethanol and ethyl acetate putting in evidence a detail showing the two non-overlapping chosen peaks: 884 cm^{-1} for ethanol and 849 cm^{-1} for ethyl acetate. The existence of strong non-overlapping peaks for the components present in the binary mixture makes this system attractive to test the Raman methodology for diffusion measurements, which was an objective of this thesis.

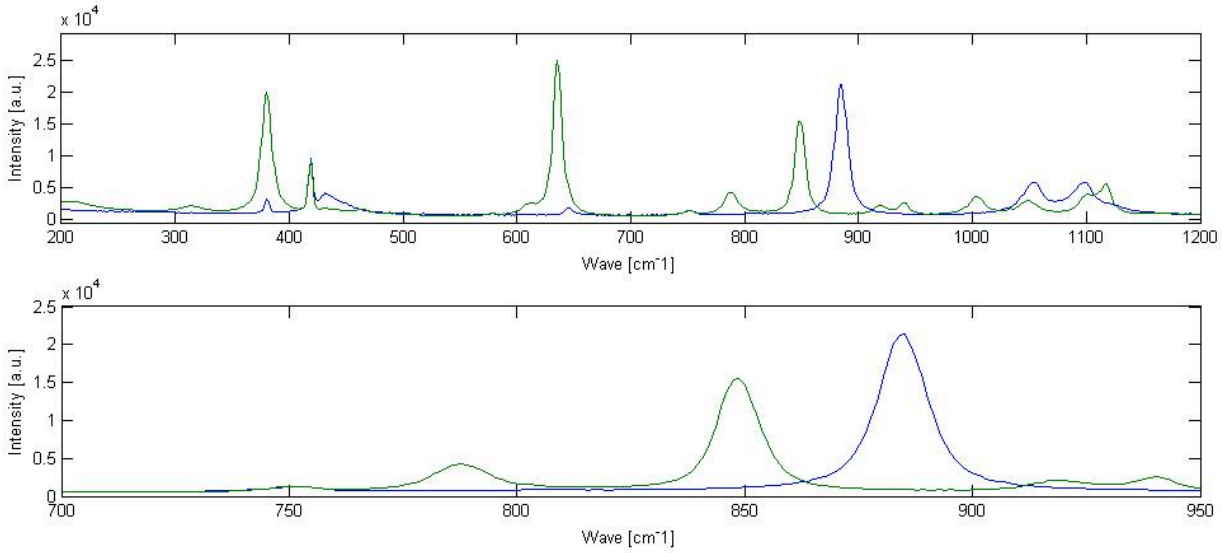

Figure 4.1 Raman spectra of pure components, ethanol (blue) and ethyl acetate (green) giving a detail of the corresponding non-overlapping peaks.

4.2 Experimental setup and procedure

The experimental setup, including the Raman instrumentation and the diffusion cell, is presented in this chapter. The special procedure used in introducing the studied solutions into the diffusion cell will also be described.

4.2.1 Raman instrumentation

A Horiba Jobin-Yvon LabRam 300 Raman microscope (figure 4.2) equipped with a liquid nitrogen cooled charge-coupled device (CCD) detector and a fiber optic probe (figure 4.3) was utilized in the diffusion study. The used laser excitation wavelength was 785 nm. The laser power in the probe was measured to be between 20 mW and 40 mW.

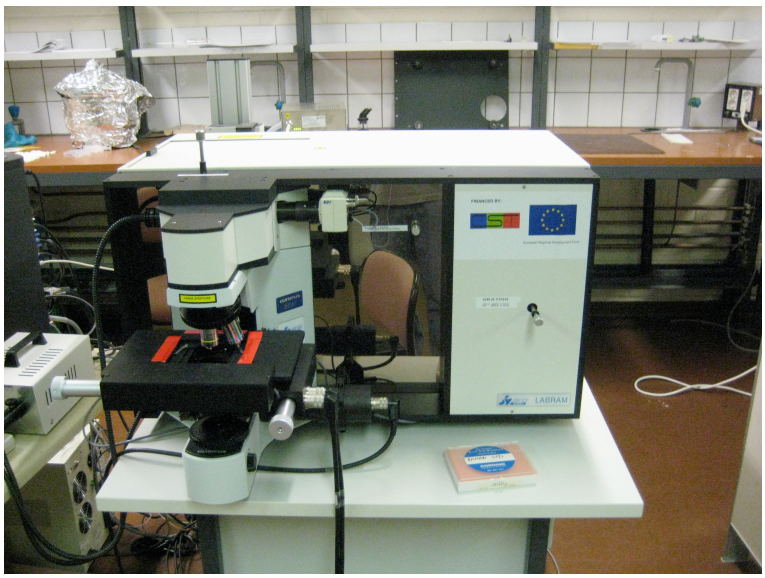

Figure 4.2 Horiba Jobin-Yvon LabRam 300 Raman microscope equipped with liquid nitrogen cooled charge-coupled device (CCD).

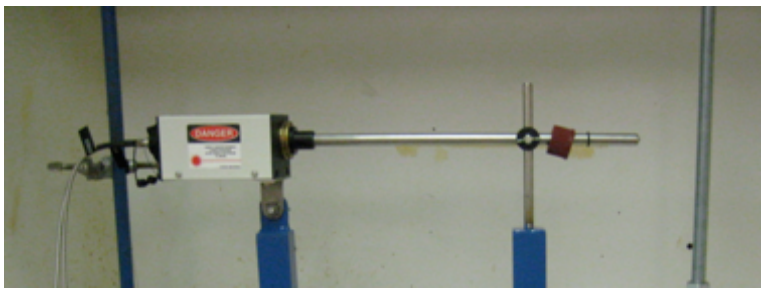

Figure 4.3 Fiber optic probe.

4.2.2 Diffusion cell and its filling procedure

Diffusion experiments were carried out in a specially designed diffusion cell made of glass as shown in figure 4.3. This diffusion cell differs from the ones used in previous works, e.g. in the works performed by Bardow's and Berg's research groups [16, 26, 28 and 29]. In the present case, the measurement was done at a fixed height (40 mm) with the Raman probe immersed into the liquid as shown in figure 4.4, not carried out through the glass wall of the diffusion cell. Measuring through glass requires utilization of a higher laser power. The experimental system was not thermostatically controlled, but the temperature in the cell was assumed to be constant since the room temperature was controlled and the laser power utilized was low.

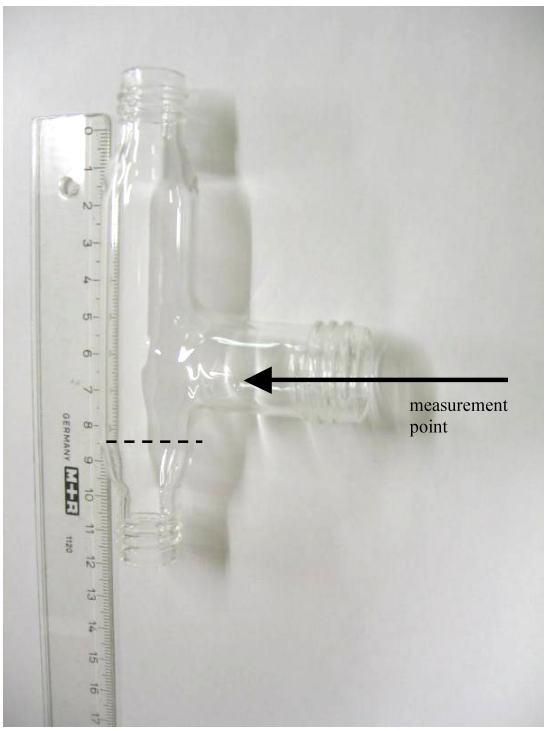

Figure 4.4 Diffusion cell used for diffusion measurements. The arrow shows the measurement point and the dashed line represents the boundary between the initial phases.

For a diffusion experiment, two solutions of different composition are used and named as the lower phase (corresponds to the solution with higher density) and the upper phase (corresponds to the solution with lower density). This procedure diminishes the gravity effect during the experiment. A second order polynomial adjustment to literature data from [31] was done in order to determine the density of the solutions. The figure 4.5 presents the linear adjustment.

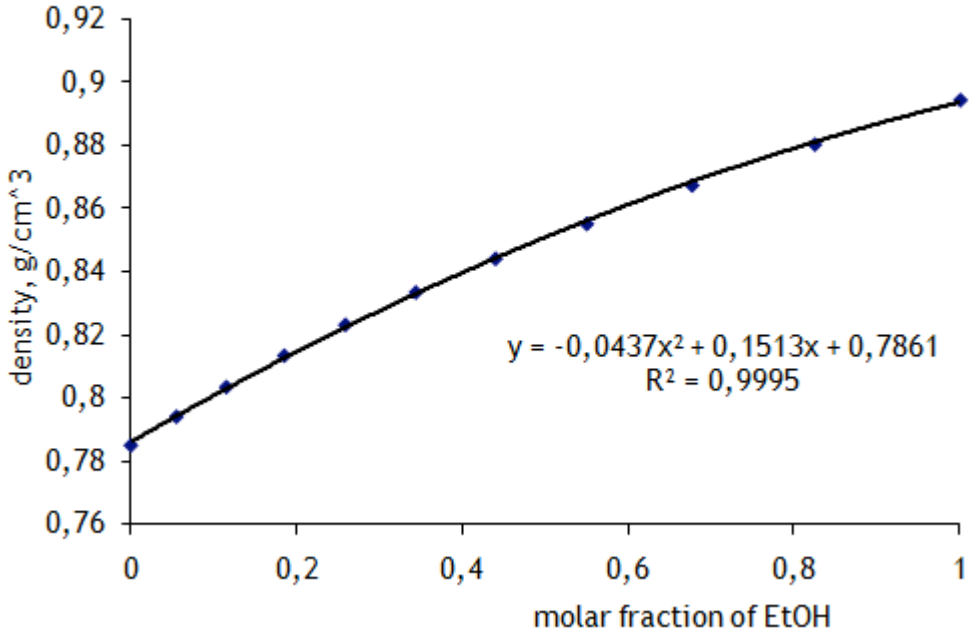

Figure 4.5 Second order Polynomial adjustment for the density and the equation fitted to the data.

The compositions of the 5 sets of diffusion measurements for an ethanol average molar fraction range between 0.4 and 0.8 are presented in table 4.2. The difference in the initial composition of the two contacting phases Δx was 0.2. The volumes of the initial lower and upper phases were 9 mL and 10 mL, respectively. The volume below the measurement point was 12 mL. The distance z between the initial boundary and the measurement point was 8 mm.

Table 4.2 Compositions of the 5 sets of diffusion measurements.

Average mol fraction		Ethanol mol fraction	
Ethanol (x_{EtOH})	Ethyl acetate (x_{EtOAc})	Upper solution	Lower solution
0.40	0.60	0.50	0.30
0.50	0.50	0.60	0.40
0.60	0.40	0.70	0.50
0.70	0.30	0.80	0.60
0.80	0.20	0.90	0.70

The mixtures were introduced in the cell using a 10 ml syringe (BD Plastipak) equipped with a specially designed polypropylene piston. During the filling step, the syringe containing the denser mixture is first placed in the bottom in standby mode (without starting the injection), and then the lighter mixture is injected from above into the cell. Only then, the denser mixture was injected slowly (injection time varied between 180 and 363 seconds) to prevent mixing from the bottom of the cell were the syringe was placed at first. A slow injection of the denser solution allowed the formation of a boundary between the mixtures at the beginning of the experiment. In order to prevent losses by evaporation, the system is closed before filling. Figure 4.6 illustrates the experiment, showing the syringes in the injection position. After the injection, the diffusion cell was carefully covered with aluminum foil in order to protect the measurement point from interfering white light.

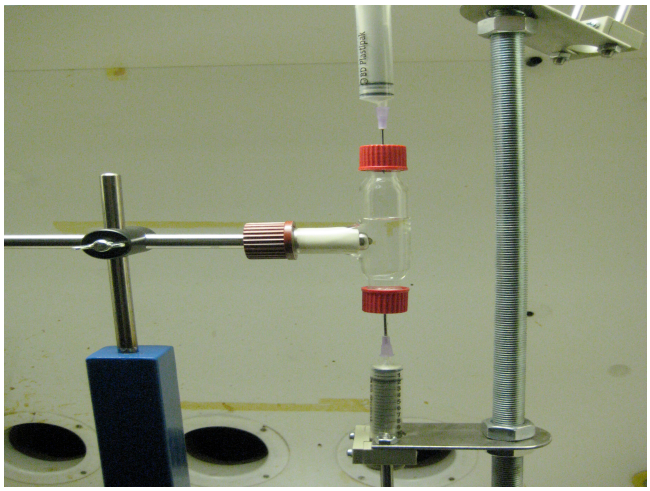

Figure 4.6 Fiber optic probe immerged, syringes on injection position and diffusion cell filled.

4.3 Acquisition of spectral data

Data acquisition was done with the help of the software LabSpec that provides a number of methods for acquiring a single spectrum. The parameters chosen for the present study are reported in this chapter.

The acquisition can be done over (1) a single shot window or (2) an extended range. In the performed experiments both approaches have been tested. Option (1) allows a shot spectrum to be acquired, with a user pre-defined integration time and averaging. Option (2) allows a spectrum to be acquired over an extended range, with a pre-defined integration time and averaging. Taking a number of individual single shot windows and “gluing” these together, it covers the extended range. The software is able to automate this procedure. In the beginning of this study, the acquisition was done over an extended range (200-1750 cm^{-1}). Afterwards,

in the final diffusion measurements, it was decided to work over a single shot window (850 cm^{-1}). The selected extended range position was comprised between 200 and 1400 cm^{-1}.

Spectrum accumulation allows spectra to be acquired with multiple accumulations and averaging. The accumulation number represents the number of individual acquisitions contributing to any particular data point in the final spectrum. The higher is this number, the longer is the acquisition time allowing the acquirement of more data points. The signal to noise ratio and the step size will be smaller. The number of accumulations used in all the experiments was 1 or 2. Figure 4.7 illustrates the effect of the accumulation number on the spectrum of pure ethanol. A significant reduction in the noise level can be seen as two accumulations are acquired instead of a single one.

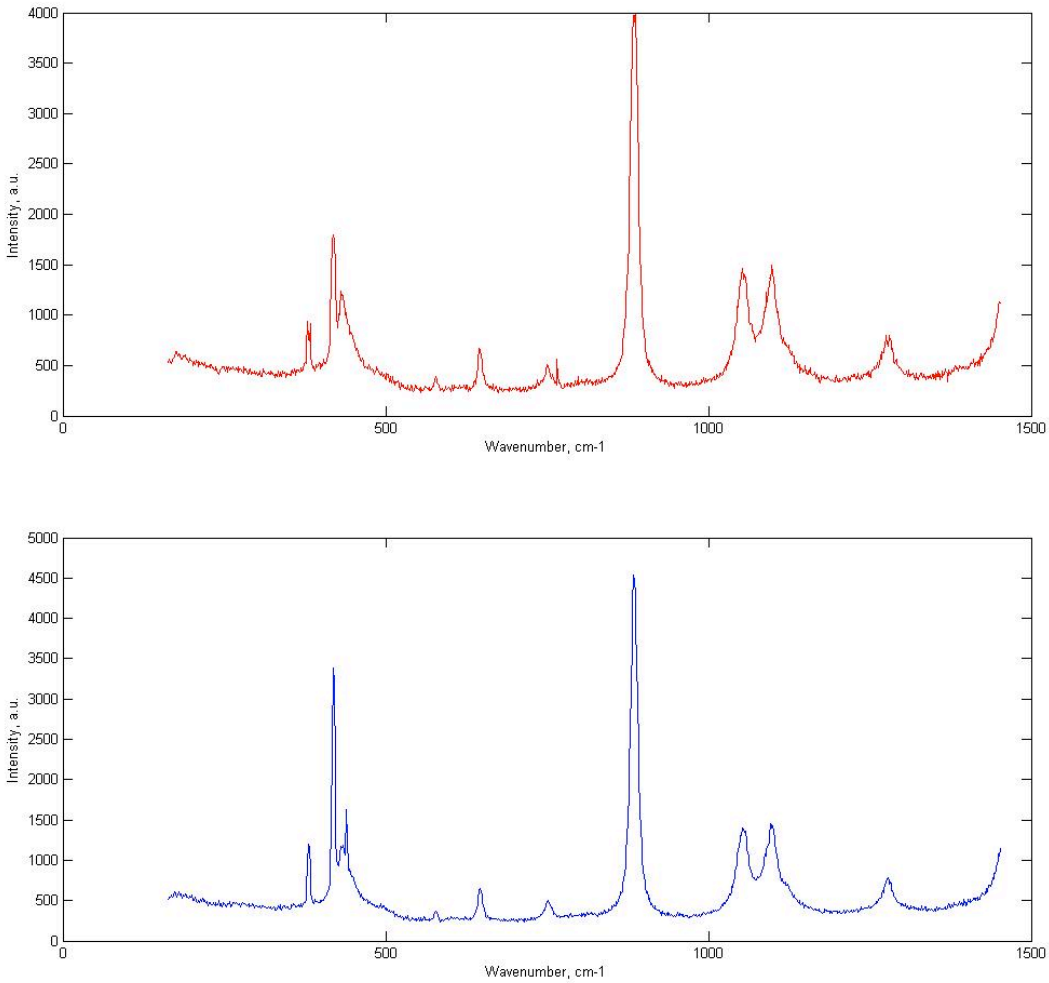

Figure 4.7 Raman spectra of pure ethanol recorded collecting 1 accumulation (red) and 2 accumulations (blue).

CCD detectors are sensitive to other forms of radiation, and in particular to random events known as cosmic rays. The cosmic rays interfere with spectra acquisition by registering very sharp and strong bands in the spectrum. Two algorithms available in LabSpec software were utilized for detecting and removing these random events. The first algorithm attempts to

locate a spike in a single accumulation and acquisition, by analysing the bands for sharpness (width) and intensity. The other, a more robust algorithm, works by comparing two accumulations within an acquisition, and thus it could be used only when the accumulation number is set greater than 2.

Integration time was another parameter that was intensively tested. In order to diminish the influence of the noise ratio, the integration time was increased from 60 to 120 seconds. Figure 4.8 shows the effect of the integration time on the spectrum of pure ethanol. It can be clearly seen, that longer integration time provides much higher intensity.

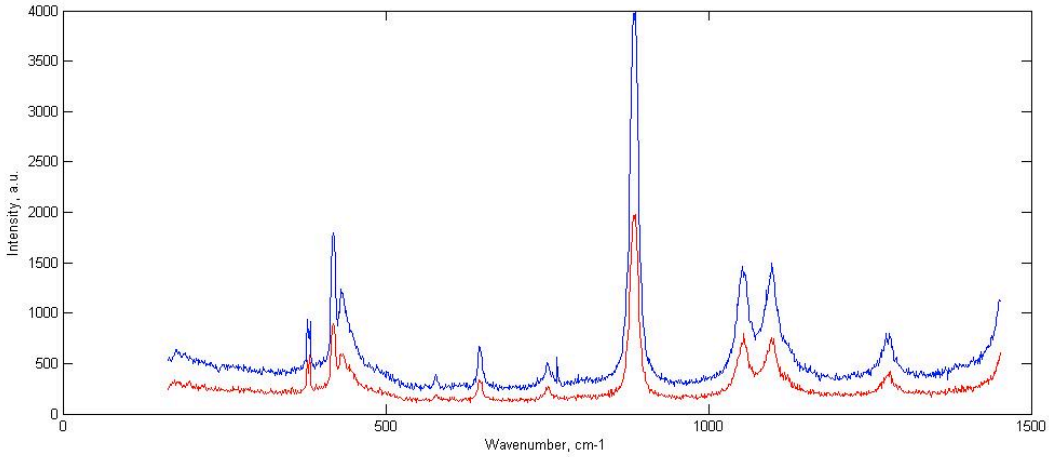

Figure 4.8 Raman spectra of pure ethanol using different integration times. The blue spectrum was recorded at 60 seconds and the red spectrum at 120 seconds.

The total measurement time in the preliminary studies was 6 hours, and a spectrum was recorded every 2 minutes. Due to the slowness of diffusion, only the very beginning of the concentration profile could be obtained during a 6-hour measurement. In order to see the development of the concentration profile more clearly, the final diffusion measurements were 24 hours. A spectrum was recorded every 3 minutes.

4.4 Data treatment

Noise in Raman spectra can be reduced with different smoothing and filtration techniques [29]. All these post treatment methods include a risk of losing some essential information, and therefore, they should only be used with discretion. This chapter describes the data treatment procedure applied in this work. The aim was to apply minimal data treatment.

Two different approaches for the determination of the composition of a mixture from the spectrum are compared in this study. The first method uses the ratio between the heights of the characteristic peaks for converting the spectral data to molar fractions. To calculate the height of a peak, a point that is representative of the valley point is subtracted from the

maximum height of the peak. The second method is based on the ratio between the areas under the peaks.

In the determination of the height of the peaks, no data treatment was performed. The ratio of the heights of the characteristic peaks showed not to be significantly influenced by the occurrence of noise in the Raman spectra. On the other hand, the areas under the peaks were considerable influenced by the noise. As so, a data treatment procedure explained next was applied.

The first step in the data treatment was baseline correction. This data analysis function available in LabSpec allows removal of the background. The type of baseline approximation used lie on polynomial curve of third degree. Figure 4.9 shows the effect of the baseline correction on the Raman spectrum of ethanol.

Another feature applied to the data treatment of the peaks was an interpolation (INTERP1 1-D interpolation) using Matlab. It interpolates using the piecewise cubic Hermite interpolation method to find values of intensity in a specific defined wavenumber array (were the peak is located). It smoothed the peaks allowing a more accurate determination that revealed to be crucial for the prediction of the diffusivities. The calculation of the area post treatment was done using equation 4.1

$$Area = \sum_{k=1}^{n}\left[\left[x(k+1)-x(k)\right]\times y(k)+0.5\times\left[x(k+1)-x(k)\right]\times\left[y(k+1)-y(k)\right]\right] \qquad (4.1)$$

x is the wavenumber (cm^{-1}) and *y* represents the intensity (a.u.). Figure 4.10 compares the EtOH peak before and after interpolation. A smoother peak shape is obtained by the data treatment.

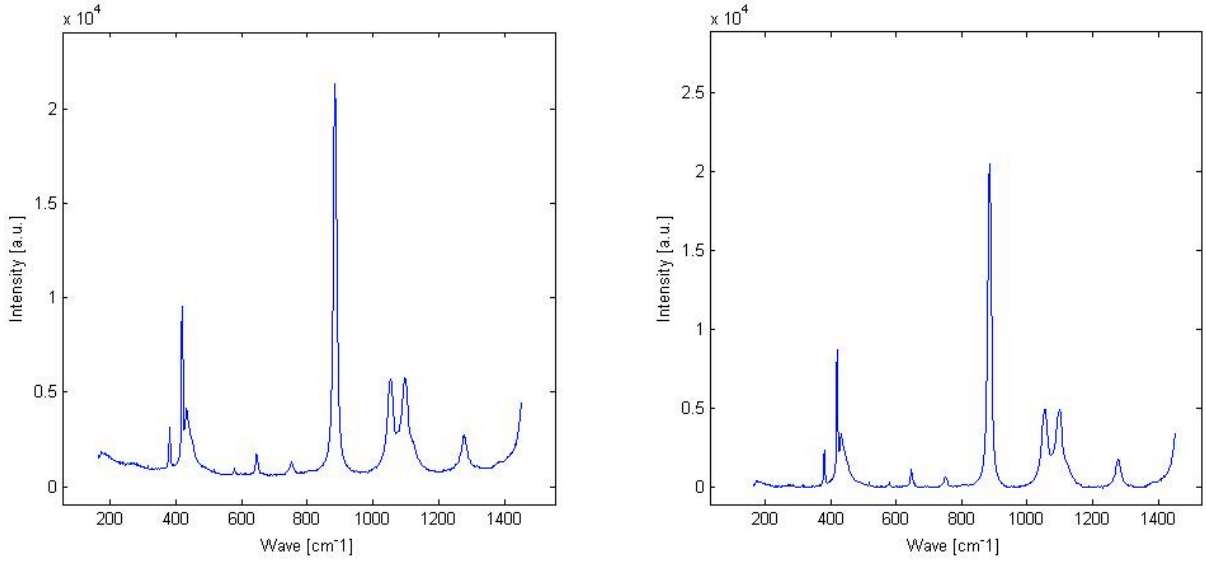

Figure 4.9 Ethanol spectra before (right) and after (left) baseline correction.

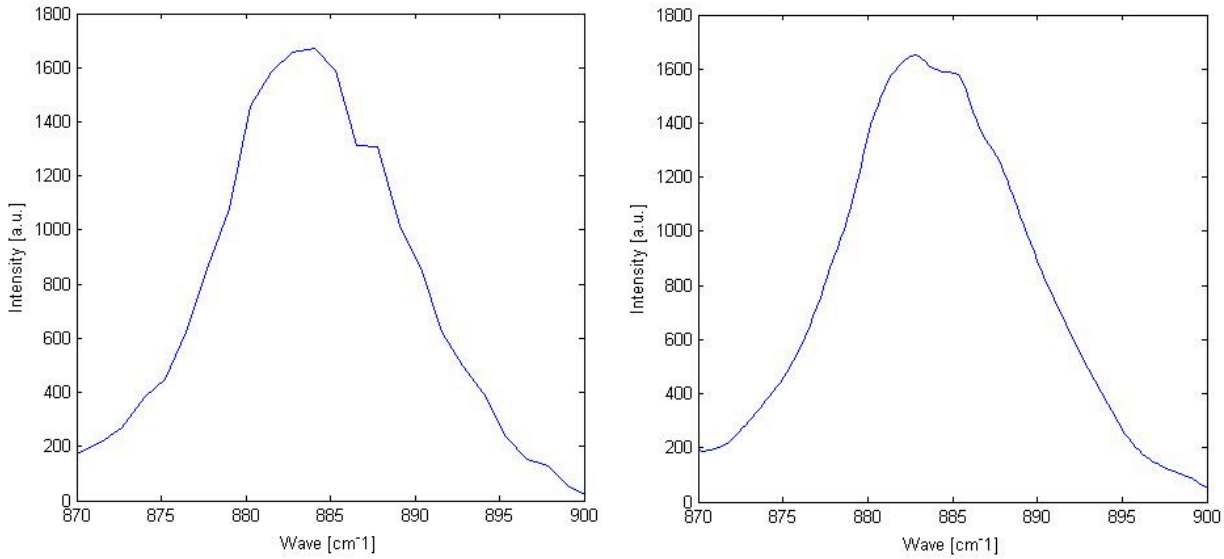

Figure 4.10 Ethanol peak before (left) and after (right) data treatment.

The calibration models applied for converting the peak heights or areas to molar fractions are explained in the next section.

4.5 Calibration procedure

The spectra of the pure solvents and several mixtures of different compositions were recorded for the calibration. The mixtures were prepared by weight using a balance with an accuracy of 0.01 g. The diffusion cell was filled with pure ethanol or ethyl acetate, or with one of the mixtures to record the spectra and obtain the calibration curve. For the calibration model, 9 mixtures of different compositions were recorded (Table 4.3).

Table 4.3 Compositions of the 9 mixtures used for the final calibration model.

m_{EtOH}, g	m_{total}, g	$x_{EtOH,}$
2.79	50.02	0.03
5.78	50.07	0.06
9.15	50.02	0.10
1.94	50.04	0.15
17.27	50.16	0.21
21.99	50.01	0.28
27.49	50.03	0.38
33.96	50.02	0.51
41.27	50.05	0.70

As described in section 4.3, different spectra acquisition parameters were tested along the study. The development of more accurate data acquisition procedures and the instability of the laser power contributed for the constant need of new calibration models along the diffusion experiments. The calibration model revealed to be very sensitive and to influence significantly the diffusion coefficients determined.

The calibration of Raman spectra can be based on the area or on the height of the characteristic peaks. Data treatment methods reported in the previous section for these two approaches, were applied for the calibration data, too. After the data treatment, linear equations 4.2 and 4.3 were fitted to the experimental data (figures 4.11 and 4.12). The fitting results are given in table 4.4.

$$X(EtOH) = a + b \times \frac{\text{peak height}(EtOH)}{\text{peak height}(EtOH) + \text{peak height}(EtOAc)} \qquad (4.2)$$

$$X(EtOH) = a + b \times \frac{\text{peak area}(EtOH)}{\text{peak area}(EtOH) + \text{peak area}(EtOAc)} \qquad (4.3)$$

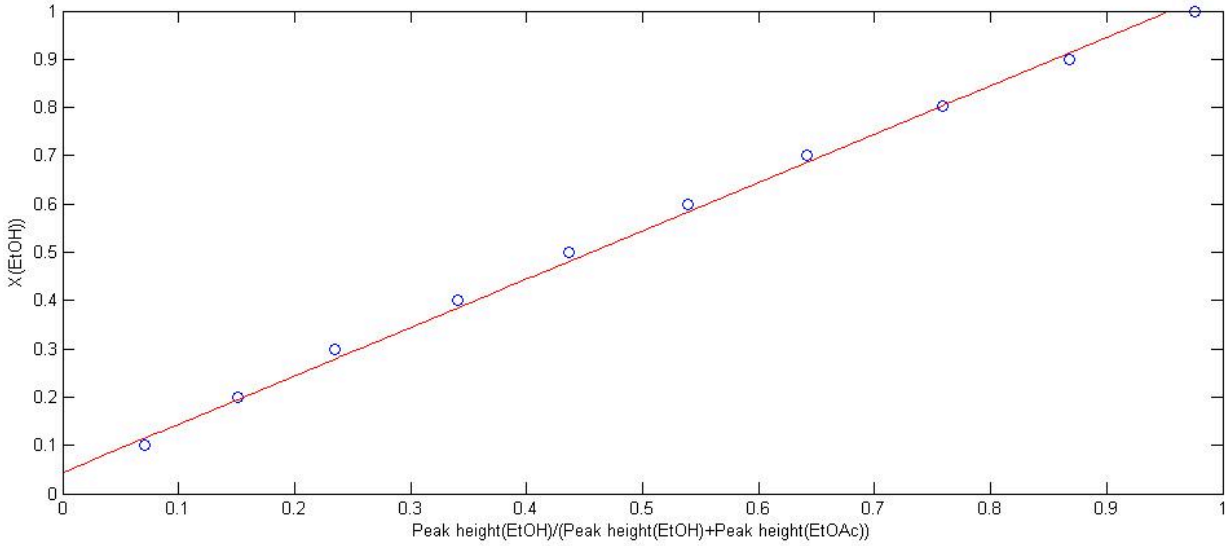

Figure 4.11 Experimental data recorded at an integration time of 120 seconds and using an accumulation number 2. Equation 4.2 fitted to the experimental data.

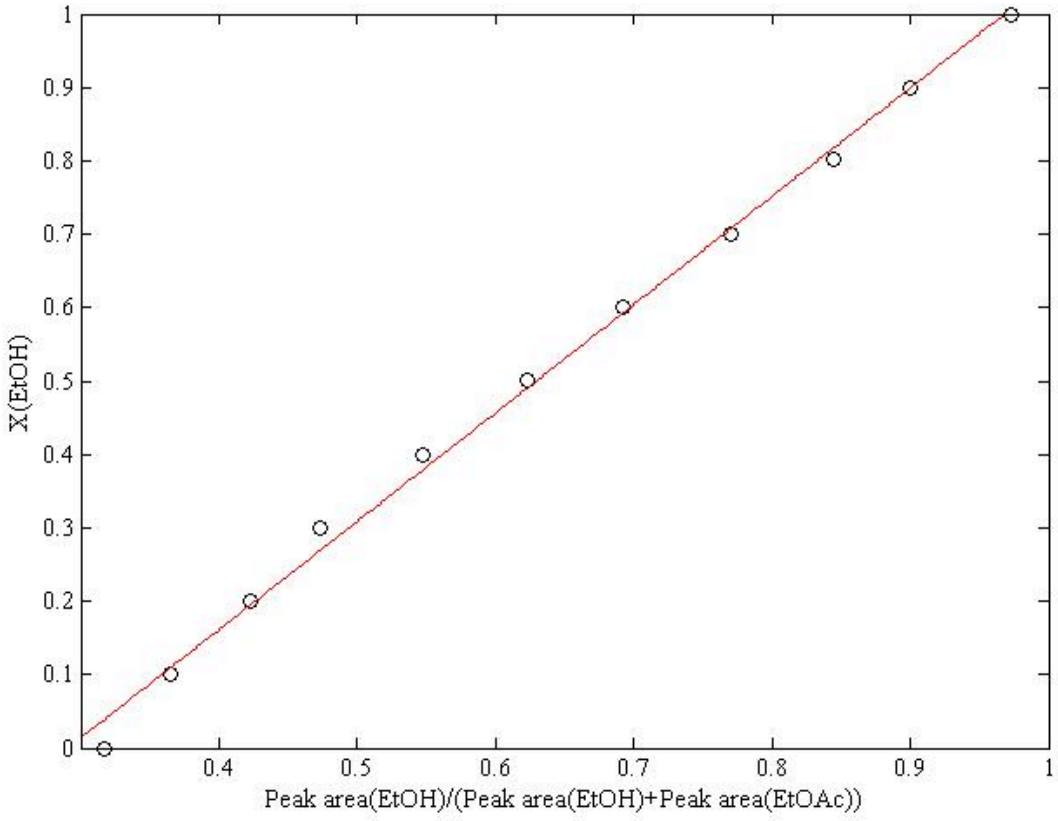

Figure 4.12 Experimental data recorded at an integration time of 120 seconds and using an accumulation number 2. Equation 4.3 fitted to the experimental data.

For the calibration based on the heights of the characteristic peaks, the linear relationship between the intensity of the signal and the composition was replaced by a quadratic

relationship (Eq. 4.4). In this case, the quadratic relationship proved to fit better the experimental data. The quadratic model did not improve the fit in the case of the peak area based model. Figure 4.13 illustrates the quadratic equation 4.4 fitted to the experimental data.

$$X(EtOH) = a + b \times \frac{\text{peak height}(EtOH)}{\text{peak height}(EtOH) + \text{peak height}(EtOAc)} + c \times \left(\frac{\text{peak height}(EtOH)}{\text{peak height}(EtOH) + \text{peak height}(EtOAc)} \right)^2 \quad (4.4)$$

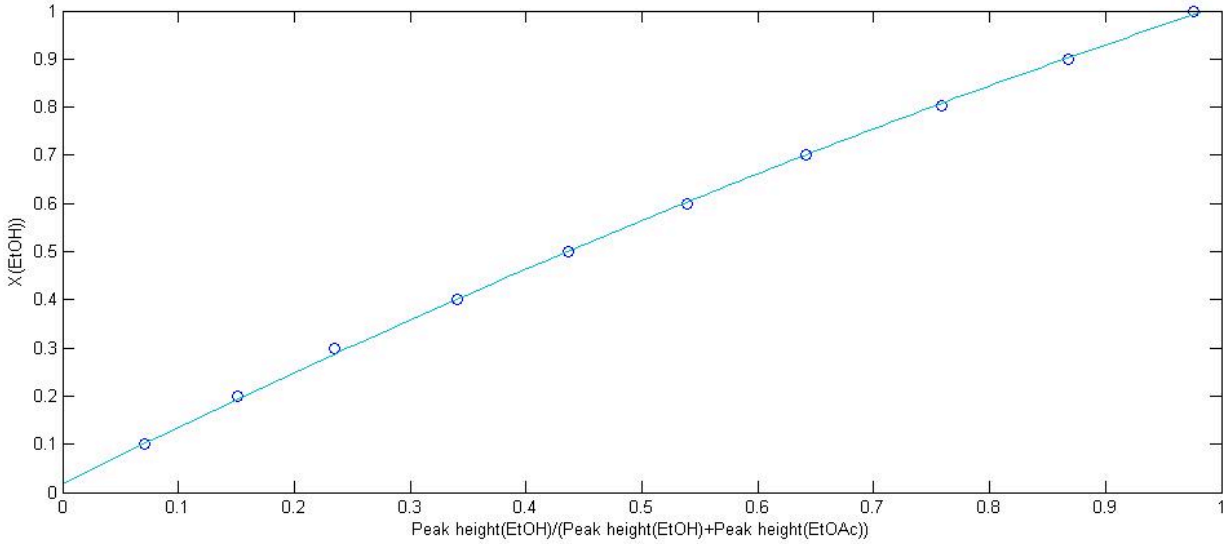

Figure 4.13 Experimental data recorded at an integration time of 120 seconds and using an accumulation number 2. Equation 4.4 fitted to the experimental data.

Table 4.4 The constants of the calibration equations.

	a	*a* t-value	*b*	*B* t-value	*c*	*c* t-value	Goodness of fit (R^2)
Linear (peak heights)	0.04	4.07	1.00	51.50	-	-	0.9966
Linear (peak areas)	-0.43	-12.01	1.5	26.84	-	-	0.9877
Quadratic (peak heights)	0.02	3.70	1.20	49.61	-0.20	-8.36	0.9996
Quadratic (peak areas)	-0.54	-12.09	1.88	12.36	-0.31	-2.66	0.9969

4.6 Diffusion models

As presented already in chapter 2, a typical way to describe diffusion is to use Fick's law (Eq. 2.1). It assumes that concentration gradient is the driving force in diffusive mass transfer. Due to its simplicity, Fick's approach was chosen as the basis of the diffusion model applied herein.

The Raman experiment data is the time profile of the concentration on a fixed height *h* in the diffusion cell. To predict the evolution of the concentration profile it has to be assumed an initially sharp concentration step [16]. The one-dimensional concentration profile evolution is based on Fick's second law (Eq. 4.5) with the necessary boundary conditions:

$$\frac{dc}{dt} = D\frac{d^2c}{dx^2}$$

$$z < 0 : c\left(z, t_{injection}\right) = c1 \qquad (4.5)$$

$$z > 0 : c\left(z, t_{injection}\right) = c2$$

where $t_{injection}$ is the time that the heaviest mixture takes to be injected into the cell and *z* the distance between the measurement point (position of the Raman probe) and the interphase. c_1 and c_2 are the initial concentrations (molar fraction) of ethyl acetate in the lower and upper phase, respectively.

Assuming that the volume of mixing is negligible, the concentrations can be directly substituted by molar fractions. This assumption was applied herein in order to simplify the

model, even though it only holds true for ideal mixtures. The molar fractions were determined from the spectral data using the calibration equations presented in chapter 1.2.2.

Method of lines approach was utilized in order to reduce the PDE into an ODE system that can be more easily solved. Matlab solver ode15s was utilized for solution. In the parameter estimation Matlab function fminsearch was utilized to minimize the sum of least squares. The Matlab code is in appendix.

Berg *et al*. [16] had solved the equation 2.2 into analytical form (Eq. 4.6)

$$c(EtOAc)(z,t) = \frac{c_1 + c_2}{2} - \frac{c_1 - c_2}{2} erf\left(\frac{z}{2\sqrt{Dt}}\right) \qquad (4.6)$$

where c_1 and c_2 are the initial concentrations (molar fractions) of ethyl acetate in the lower and the upper phase, respectively, $c(EtOAc)(z,t)$ is the molar fraction of ethyl acetate at distance z between the interphase and the measuring point at time t, *erf* is the error function, and D is the Fick's law molar diffusion coefficient.

Equation 4.6 is valid assuming that: (1) the upper and lower boundary conditions are not influenced (the assumption of infinitely thick layers), and (2) the concentration step has to be sharp as possible when the experiment starts [16]. The numerical method of lines based solution and the one calculated from equation (4.6) were compared.

4.7 Predictive methods

The established diffusivity measurements are considered laborious and time consuming. Few systems have been studied and even fewer have been studied by Raman spectroscopy [16]. The available data on diffusion coefficients is scarce. For this reason, no literature values of diffusivity for the liquid ethanol + ethyl acetate system were found. The impossibility to compare the obtained results with literature values motivated the use of predictive models introduced in chapter 2. The present chapter gives the results obtained. Next, in chapter 5, the predicted values will be compared with the experimental data.

Methods formulated to estimate the diffusion coefficient at infinite dilution were applied. The methods and its respective results are listed in table 4.5. All the physical properties used are reported in table 4.1.

Table 4.5 Diffusivities of ethyl acetate in ethanol at infinite dilution calculated using different predictive methods.

Method	Diffusivity, cm^2/mol
Scheibel	2.21×10^{-5}
Wilke-Chang	9.22×10^{-6}
Tyn-Calus	1.11×10^{-5}
Modified Tyn-Calus	8.44×10^{-6}
Hayduk-Minhas	8.93×10^{-6}
Modified Hayduk-Minhas	8.93×10^{-6}

In Scheibel method, the constant *A* was considered equal to 1.75×10^{-7} [2]. In Wilke-Chang method, if the solvent is ethanol, it is recommended to use ϕ equal to 1.5 [3]. In Tyn-Calus and Hayduk-Minhas methods, the parachors (*P*) are related with the liquid surface tension (Eq. 2.15) [3].

As already stated, the above-mentioned methods are limited to infinitely dilute solutions. Therefore they are not applicable to be compared with the diffusivities measured in concentrated solutions using Raman spectroscopy. Vignes approach (Eq. 2.22) was considered to correlate the composition effect. The thermodynamic factor *a* was calculated using the Non-Random Two Liquid (NRTL) model (Eq. 2.23) and Wilson equation (Eq. 2.24). Wilson and NRTL parameters were given by [32] and [33]. Figure 4.14 and table 4.6 present the obtained results. The diffusion coefficients at infinite dilution used in equation 2.22 were estimated by Hayduk-Minhas method, and the obtained values are presented in table 4.6. The diffusivities at infinite dilution were estimated by Hayduk-Minhas method. The value of the diffusivity of ethyl acetate in ethanol is 8.93×10^{-6} cm^2/s and the value of the diffusivity of ethanol in ethyl acetate is equal to 3.53×10^{-5} cm^2/s.

Table 4.6 Predicted diffusivities. D_1 using NRTL equation and the parameters given in [32]. D_2 predicted using NRTL equation and the parameters reported in [33]. D_3 predicted using Wilson equation and the parameters of [32]. a_1, a_2 and a_3 are the thermodynamic factors, respectively.

x_{EtOH}	α_1	D_1, cm^2/s	α_2	D_2, cm^2/s	α_3	D_3, cm^2/s
0.400	0.9999995	2.04×10^{-5}	0.579	1.18×10^{-5}	0.633	1.29×10^{-5}
0.498	0.9999995	1.78×10^{-5}	0.562	1.00×10^{-5}	0.614	1.09×10^{-5}
0.601	0.9999995	1.55×10^{-5}	0.579	8.95×10^{-5}	0.625	9.67×10^{-5}
0.700	0.9999996	1.35×10^{-5}	0.630	8.49×10^{-6}	0.668	9.01×10^{-6}
0.801	0.9999997	1.17×10^{-5}	0.717	8.42×10^{-6}	0.744	8.74×10^{-6}

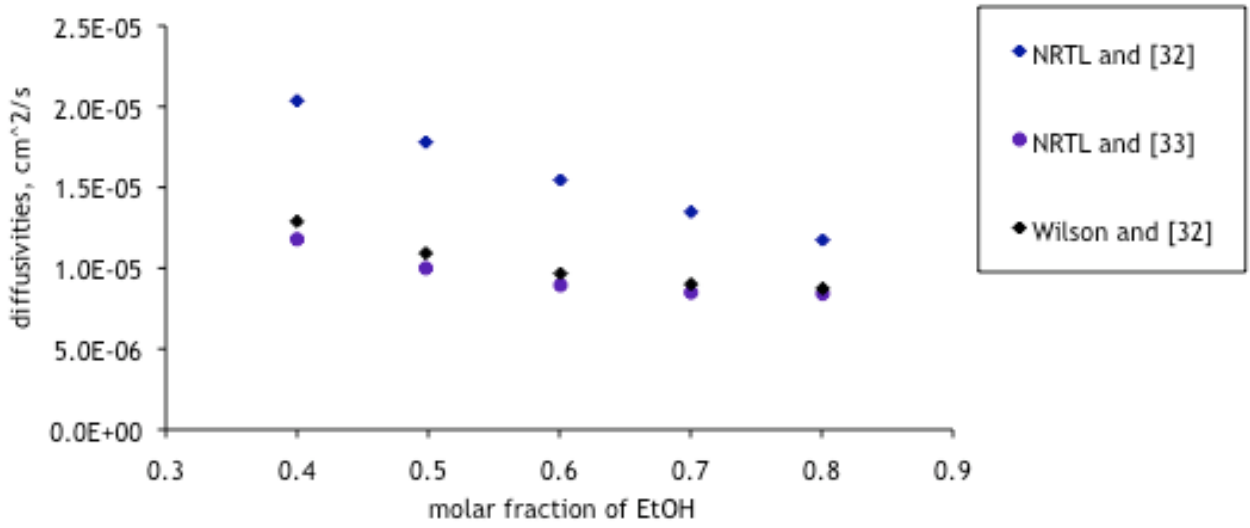

Figure 4.14 Diffusion coefficients predicted for different solute (ethanol) concentrations using 3 different methodologies

5 Results and discussion

In this chapter the results obtained for the diffusion coefficient measurements are presented and discussed. Firstly, the experimentally acquired spectra are given. Then, the diffusivities estimated using models based on the peak height and on the peak area are presented and thereafter compared. In the absence of literature data, the predictive models were used to evaluate the experimentally estimated values. Finally, a discussion concerning the use of the Raman methodology is given.

5.1 Diffusion of ethyl acetate in ethanol

As previously described in chapter 4, Raman spectrometer was utilized for monitoring the concentration profile during the diffusion experiments. The changes occurring in the Raman spectrum were recorded at constant time intervals and with the Raman probe positioned at a fixed height in the diffusion cell. A typical record is illustrated in figure 5.1. For the characteristic peaks of ethanol (885 cm^{-1}) and ethyl acetate (848 cm^{-1}) one may observe respectivelly, an increase and a decrease in the peak height with time.

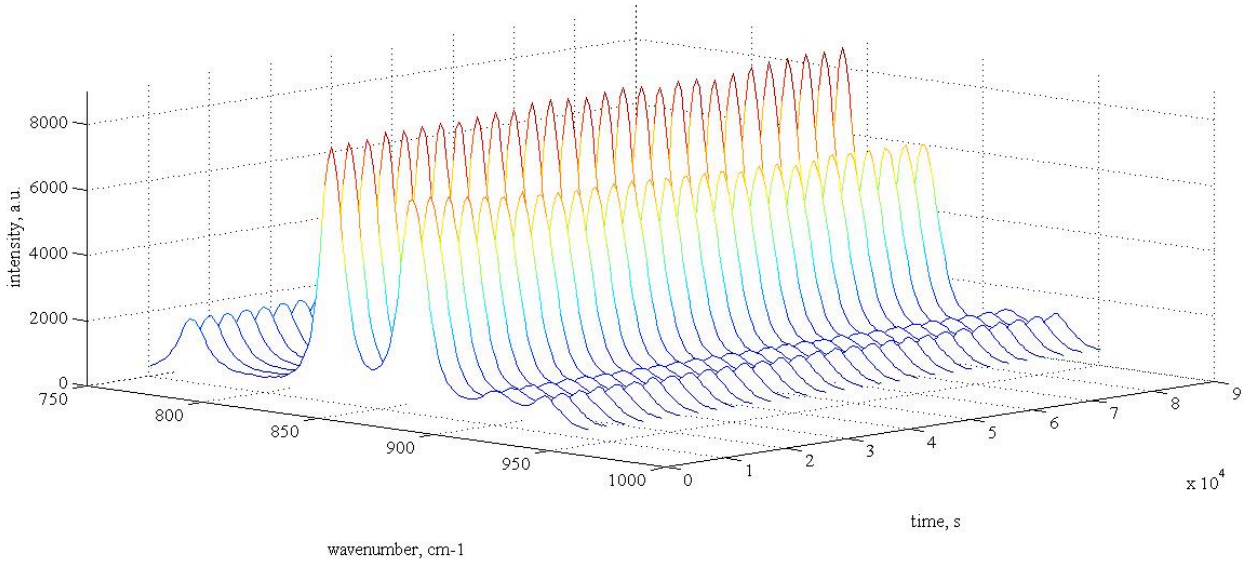

Figure 5.1 Profile evolution of the Raman spectra with time recorded at a fixed observation level during a diffusion experiment (average composition of ethanol equal to 0.4).

Prior to the determination of the diffusion coefficients, the spectral data had to be converted into molar fractions of the two components. In this study two different approaches regarding the determination of the molar fraction from the obtained spectral data were used: (1) the ratio between the heights of the two characteristic peaks and, (2) the ratio between the areas under the two characteristic peaks. A detailed description of these methods was given

in chapter 4. In this chapter, the results obtained using these two approaches will be presented separately.

To predict the evolution of the concentration profile, two approaches were considered, the first, based on Fick's second law, respecting the boundary conditions given in equation 4.5 and assuming ideality; the second, was based on the analytical solution of equation 4.5 (eq. 4.6) given by Berg *et al*. [16] assuming infinitely thick layers. Additional information of the used approaches is described more detailed in chapter 4. The diffusion coefficient data presented in table 5.1 is estimated using the method based on peak height. Table 5.2 presents the diffusion coefficients determined using the areas of the characteristic Raman bands of ethanol and ethyl acetate.

Table 5.1 Diffusion coefficients data using the peak heights. D_a is based on Fick's second law. D_b is obtained using equation 4.6.

$x_{Ethanol}$	D_a (cm^2/s)	D_b (cm^2/s)
0.40	2.50×10^{-5}	2.69×10^{-5}
0.50	1.80×10^{-5}	1.94×10^{-5}
0.60	1.55×10^{-5}	1.59×10^{-5}
0.70	1.33×10^{-5}	1.59×10^{-5}
0.80	1.23×10^{-5}	1.31×10^{-5}

Table 5.2 Diffusion coefficients data using the area under the peaks. D_a is based on Fick's second law. D_b is obtained using equation 4.6.

$x_{Ethanol}$	D_a (cm^2/s)	D_b (cm^2/s)
0.40	4.75×10^{-5}	5.34×10^{-5}
0.50	1.20×10^{-5}	1.26×10^{-5}
0.60	5.00×10^{-6}	5.38×10^{-6}
0.70	3.06×10^{-6}	3.22×10^{-6}
0.80	1.38×10^{-6}	1.42×10^{-6}

The comparison between the results obtained using the two methods are presented in figure 5.2. In general the determined diffusivity values using the peak height based method are higher than the corresponding ones based on the area method. However, one exception was found when using an average molar fraction of ethanol equal to 0.4 where the tendency diverges from the rest of the results.

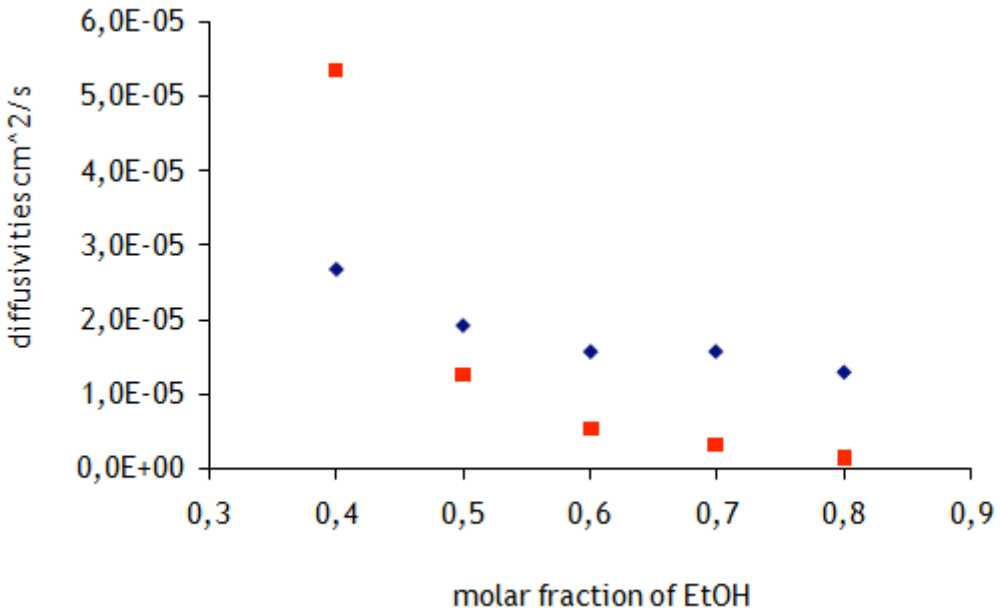

Figure 5.2 Diffusion coefficients obtained using the method of lines. Blue points and red points are based on peak height and peak area approaches, respectively.

The diffusion profiles based on the peak heights are shown in figure 5.3 (concentration profiles in the cell as a function of time) and in figure 5.4 (time profile of concentration at the measuring point). These profiles were obtained for the average molar fraction of ethanol equal to 0.8.

The diffusion profiles based on the areas under the peaks are not presented since they are not very illustrative. The efforts conducted to improve the calibration model or the data treatment did not produce results with sufficient reliability to be presented and compared with the diffusion profiles based on the peak heights.

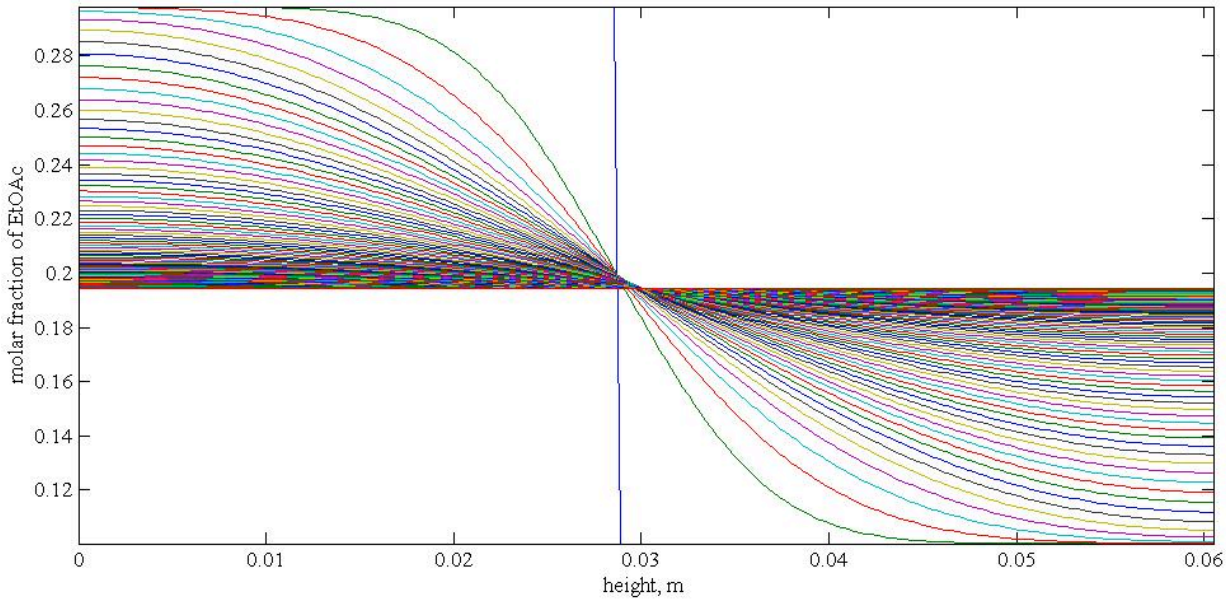

Figure 5.3 Concentration profiles in the cell at different time points.

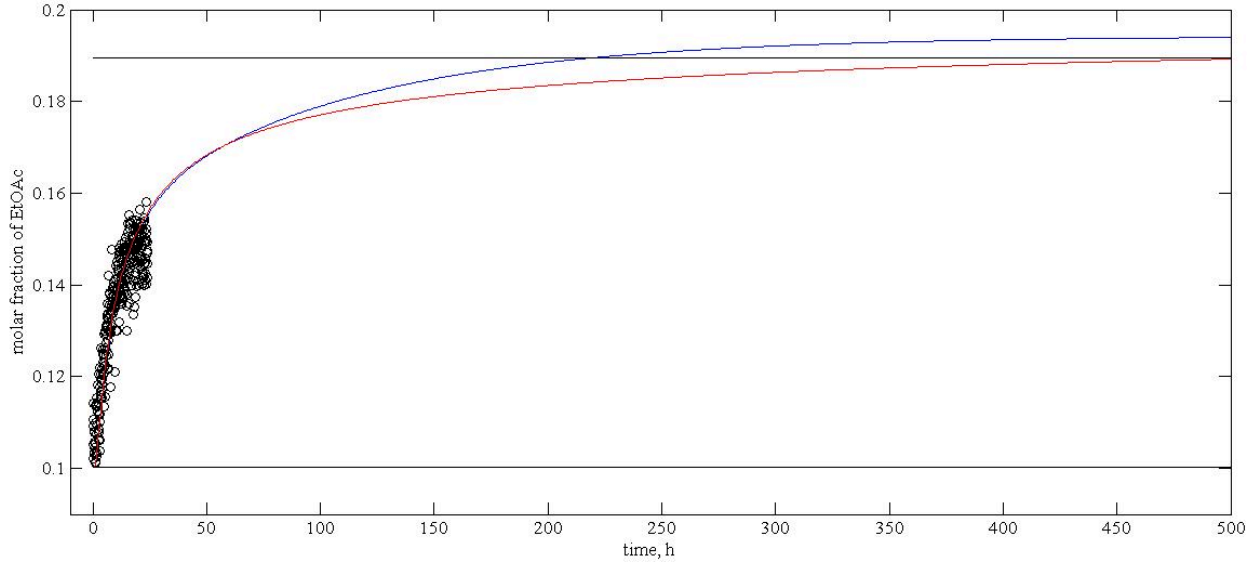

Figure 5.4 Time profile of the molar fraction of ethyl acetate at the monitoring point. Experimental data is presented with black rings. Blue curve is the model solved using method of lines and the red one using equation 4.7. Horizontal lines represent the initial and the calculated concentrations for infinite time.

5.2 Comparison between the predicted and measured diffusion coefficients

Predictive methods for estimation of diffusion coefficients were presented in chapter 2. Now, the experimental results are compared with the diffusion coefficient predictions presented in chapter 4. The predicted values are compared with both approaches: (1) based in the peak heights, and (2) based on the areas under the peaks. Figure 5.5 gives the plot of the diffusivities predicted and the experimental values determined using the approach based on the peak heights.

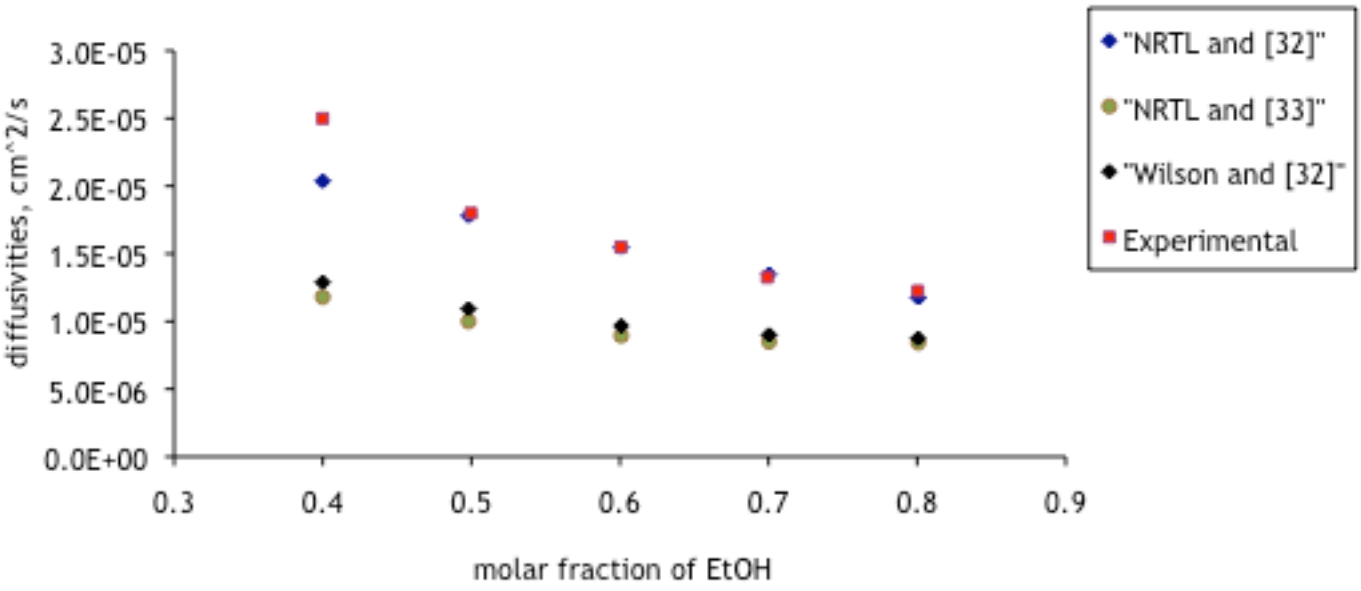

Figure 5.5 Diffusivities comparison. Experimental data is presented in red. In blue, diffusivities predicted using NRTL equation and the parameters given in [32]. Diffusivities predicted using NRTL equation and the parameters reported in [33] are presented in green. In black is presented the predicted diffusivities using Wilson equation and the parameters in [32].

From figure 5.5, it is clear that the experimental diffusion coefficients are in the best agreement with the diffusion coefficients predicted using NRTL equation and using the parameters given in [32].

The best fit came out with a diffusion coefficient of 1.55×10^{-5} cm^2/s. This value of diffusivity, plotted at the average composition of ethanol equal to 0.6.

The results based on the areas under peaks are now presented. Figure 5.6 gives a comparison between the estimated and the predicted diffusivities. As previously mentioned, this approach did not produce successful diffusion profiles. As expected and proven in figure 5.6,

it is difficult to state that this estimations fitted any particular prediction method or thus select a best fit plotted at any composition.

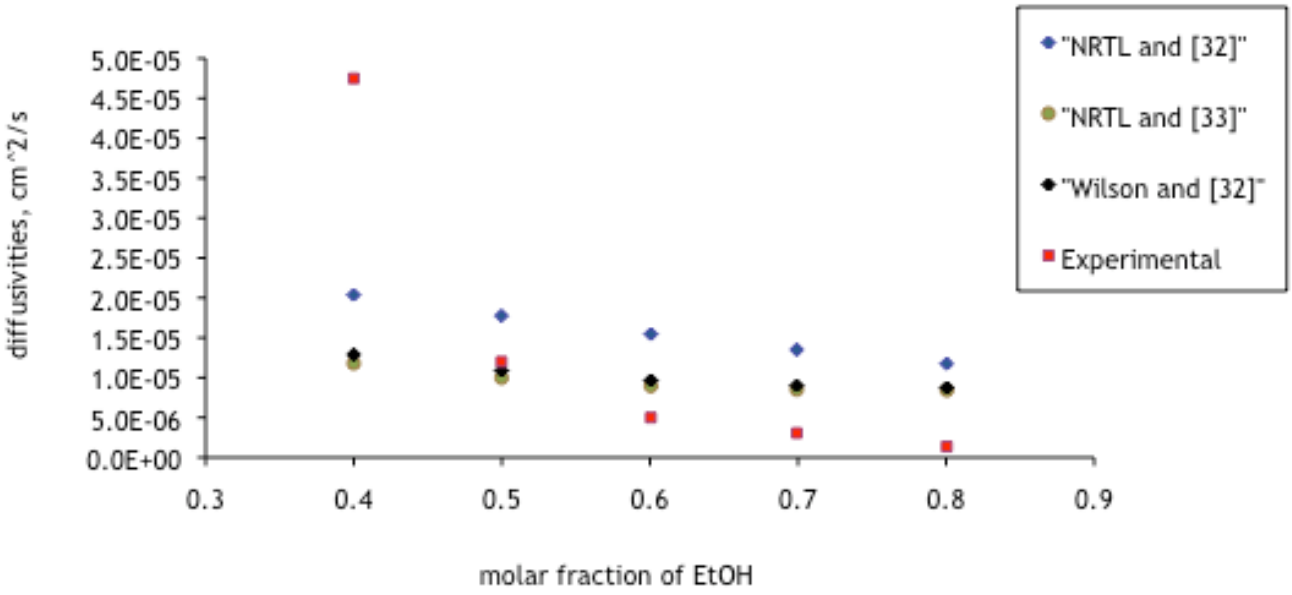

Figure 5.6 Diffusivities comparison. Experimental data is presented in red. In blue, diffusivities predicted using NRTL equation and the parameters given in [32]. Diffusivities predicted using NRTL equation and the parameters reported in [33] are presented in green. In black is presented the predicted diffusivities using Wilson equation and the parameters in [32].

5.3 Evaluation of the Raman method

By making changes to the experimental and model design, the diffusivities obtained in this study showed to change considerably. The tested acquisition options, the increase of the intensity of the laser power and the improvement of the injection procedure allowed the diffusivities estimation.

The optimization of the laser power proved to be crucial to generate significant improvements. The increase of the laser power contributed for the estimation of reliable results. In the model based on the peak heights it decreased the influence of the noise in the spectra significantly producing reliable results.

As the acquisition time is lengthened to 120 seconds, the intensity increases. Short acquisition times are preferred for non steady state systems, but the experiment duration of 24 hours assured a sufficiently high number of data point even with higher acquisition times.

When using the model based on the peak heights, the optimization of the laser power and the increase of the acquisition times proved to generate accurate diffusivities estimations without the need to use post-processing of the data.

For the model based on the areas under the peaks, the improvements caused by the optimization of the laser power and increasing of the acquisition times weren't sufficient to generate satisfactory estimations. The data treatment described in chapter 4 contributed for a significant improvement but, it wasn't enough to generate satisfactory estimations to be compared with the ones estimated by the model based on the peak heights. The quality of the peaks shapes after the data treatment revealed to be insufficient to estimate accurate areas values.

Using the model based on the peak heights, at an ethanol average composition of 0.6 was plotted the diffusivity in best agreement with the predicted values. The composition range in best agreement with the predicted results is from 0.5 to 0.7. The compounds that constitute the system influence the composition range that can be studied, since the ratios of the heights/areas of the characteristic peaks at different concentrations are dependent on the components (on their Raman spectra). When the peak heights/area of the two components are almost equal (height/area ratio about 1:1), the level of noise is higher. In the studies by Berg *et al.*, the best fit plotted at the average composition 0.47 [16] and Bardow *et al.* conclude that the concentration dependency of the binary diffusivities delivers accurate estimations in the composition interval from 0.2 to 0.85 mol [27].

6 Conclusions and future work

Measuring diffusion coefficients trustworthy and reliably is reputed to be difficult. The available data on diffusion coefficients, even for binary mixtures, is scarce. Moreover, as far as we know, for the binary system tested in this work (ethanol + ethyl acetate) no data have been published yet.

Diffusion in liquids is a very slow process and experimental studies are in general characterized to be complex and time-consuming. A number of experiments are needed for the determination of multicomponent diffusion coefficients, even for a single composition. In such context, Raman is a viable methodology since it can overcome some of the typical drawbacks of the conventional methods. It enables direct and simultaneous determination of concentrations in multicomponent mixtures. Moreover, it allows fast measurements.

Based on these advantages, a novel procedure to study diffusion using model-based Raman spectroscopy has been developed, the pioneer groups being the ones of Bardow [26, 28 and 29] and Berg [16]. This methodology can be used to obtain liquid concentration data for binary and multicomponent mixtures enabling the establishment of the evolution of the corresponding concentration profiles with time. The developed methodology showed that reproducible results on diffusion measurements can be obtained using a single experiment. Face to the mentioned potentialities, every work on diffusion study using Raman technique constitutes an important contribution for further development of the technique.

In this work the model-based Raman spectroscopy methodology was implemented at the Department of Chemical Technology at Lappeenranta University of Technology. The experimental set-up includes a Raman spectrometer (equipped with a fiber optic probe and a diffusion cell. Comparatively to the previously published work of Bardow's and Berg´s research groups, this cell enables the direct immersion of the probe into the liquid improving the output signal even with the use of a lower laser power source. The laser power proved to be an important parameter to optimize in order to achieve a suitable signal to noise ratio. The experimental procedure being comprised of cell filling, calibration and diffusion measurements was done with success using the binary mixture of ethanol and ethyl acetate. In conclusion, the experimental set-up proved to be adequate to perform diffusion studies and could be extended to study other systems (binary and multicomponent). One requisite must, however, be observed: the individual spectra of the components must present a non-superimposing peak to enable concentration determination.

Data acquisition was done with the software LabSpec and some acquisition parameters have been optimized. In the final diffusion measurements a single shot window (850 cm^{-1}) and an

extended range position comprised between 200 and 1400 cm^{-1} were used. A significant reduction in the noise level was obtained using two accumulations instead of a single one.

In order to determine the composition of the mixture from the spectral data, two different approaches were tried. The first method was based on the peak height and the second one on the peak area. The first one proved to be less influenced by the noise associated to the Raman spectra and was the preferential method chosen in this work (spectra data could be used as such without any previous manipulation). Some efforts have been used to increment the quality of the peak area method namely by performing additional data treatment (base line correction and smoothing) before area determination. Further work is needed in order to improve the peak area method that could even involve the increment of the laser power (noise reduction).

This study shows that time-dependent concentration profiles during inter-diffusion experiments are liable to be determined experimentally. The two approaches used to fit the concentration profile, the one based on the numerical resolution of the Fick's second law and the one based on its analytical solution proved to generate reliable diffusion coefficients values. Furthermore, the obtained diffusion coefficients are in agreement with the diffusion coefficients predicted by the predictive methods. The estimated value for the diffusivity of ethyl acetate in ethanol was 1.55×10^{-5} cm^2/s. This value was obtained using the peak height approach and Fick's second law. The study showed that the ethanol composition molar fraction interval from 0.5 to 0.7 generates the most accurate results, i.e. it presents better agreement with the values generated by the predictive models.

The primary way to improve the accuracy and reliability of the results is to reduce the noise level by optimizing the measurement parameters and developing the data treatment procedure. Other improvements to the present work could include: (1) development of a temperature-controlled cell to study the temperature dependency of diffusion coefficients, and (2) development of a diffusion cell that enables the measurement at different cell position instead of the cell with a fixed position used in this work.

Raman spectroscopy is a very promising method for conducting diffusion studies. Further studies using different binary and multicomponent systems are, however, needed in order to consolidate and spread the methodology.

7 References

1. D. Bosse, *Diffusion, viscosity and thermodynamics in liquid systems*, PhD Thesis, Kaiserslautern University of Technology, 2005.
2. E.L. Cussler, *Diffusion: Mass Transfer in Fluid Systems*, 2nd ed. Cambridge, 1997.
3. B.E. Poling, J.M. Prausnitz, J.P. O'Connell, *Properties of Gases and Liquids*. 5th ed. New York, McGraw-Hill, 2001.
4. M. Koiwa, Historical development of diffusion studies, Metals and materials, Vol. 4, 6 (1998), 1207-1212.
5. R. Krishna, J.A. Wesselingh, *Mass Transfer in Multicomponent Mixtures*, 1st ed. Delft University Press, 2000.
6. V.K. Chhaniwal, A. Anand, C.S. Narayanamurthy, Measurements of diffusion transparent liquid solutions using Michelson interferometer, *Optics and laser in Engineering* 42 (2004), 9-20.
7. W.A. Wakeham, J. Kestin, *Transport properties of fluids: Thermal conductivity, viscosity, and diffusion coefficient*, Vol. I-1, Purdue Research Foundation, United States of America, 1988.
8. J. Millat, J.H. Dymond, C.A. Nieto de Castro, Transport properties of fluids: Their correlation, prediction and determination, Cambridge University Press, 1995.
9. A. Anand, V.K. Chhaniwal, S. Mukherjee, C.S. Narayanamurthy, Diffusion studies in liquids by multiple beam interferometer, *Opt Laser Technol*, 33 (2002), 45-9.
10 I.M.J.v.d. Ven-Lucassen, F.G. Kieviet, P.J.A.M. Kerkhof, Fast and convenient implementation of the Taylor dispersion method, *J. Chem. Eng. Data*, vol. 40 (1995) 2, 407-411.
11. R.C. Reid, T.K. Sherwood, J.M. Prausnitz, *Properties of Gases and Liquids*. 3rd ed. New York: McGraw-Hill, 1977.
12. S.H. Chen, H.T. Davis, D.F. Evans, *The Mathematical Theory of Non-Uniform gases*, 3rd ed. Cambridge University Press, 1970.
13. O.R. Quayle, The parachors of organic compounds: An interpretation and catalogue, 53 (1953), 439.
14. E. Smith, G. Dent, *Modern Raman spectroscopy: A practical approach*, John Wiley & Sons, England, 2005.

15. Y. Ozaki, S. Šašic, Introduction to Raman Spectroscopy, in *Pharmaceutical Applications of Raman Spectroscopy*, John Wiley & Sons, New Jersey, 2008, p. 7.

16. R.W. Berg, S.B. Hansen, A.A. Shapiro, E.H. Stenby, Diffusion Measurements in Binary Liquid Mixtures by Raman Spectroscopy, *Applied Spectroscopy*, 61 (2007) 4, 367-373.

17. The Nobel Foundation**, (**http://nobelprize.org/nobel_prizes/physics/laureates/1930/), 5.8.2009

18. S. Morel, F. Adar, Refined Raman spectroscopy: Bringing new insight into industrial processes, Optic & Photonics news, *Optical Society of America*, 2005.

19. R.L. McCreery, Instrumentation for Dispersive Raman Spectroscopy. in Laserna, 1996, pp.51-55.

20. University of Cambridge: Raman spectroscopy, (http://www.msm.cam.ac.uk/doitpoms/tlplib/raman/index.php), 6.8.2009

21. J.J. Laserna, *Modern techniques in Raman spectroscopy*, John Wiley & Sons, 1996.

22. I.R. Lewis, G.M. Howell, *Handbook of Raman spectroscopy*, Marcel Dekker, New York, 2001.

23. D.G. Miller, J.G. Albright, R. Mathew, C.M. Lee, J.A. Rard, L.B. Eppstein, Isothermal diffusion-coefficients of NaCl-MgCl2-H2O at 25 degrees-C. 5. Solute concentration ratio of 1/1 and some Rayleight results, *J. Phys. Chem.*, 97 (1993), 3885.

24. D.G. Leaist, Determination of ternary diffusion coefficients by the taylor dispersion method, *J. Phys. Chem.*, 94 (1990), 5180.

25. A. Bardow, W. Marquardt, V. Göke, H.-J. Koss, K. Lucas, Model-Based Measurement of Diffusion Using Raman Spectroscopy, *AIChE Journal*, 49 (2003) 2, 323-334.

26. R. Taylor, R. Krishna, *Multicomponent mass transfer*, John Wiley & Sons, New York, 1993.

27. A. Bardow, V. Göke, H.-J. Koß, K. Lucas, W. Marquardt, Concentration-dependence diffusion coefficients from a single experiment using model-based Raman spectroscopy, *Fluid Phase Equilibria*, 228-229(2005), 357-366

28. E. Kriesten, M.A. Voda, A. Bardow, V.Göke, F. Casanova, B. Blümich, H.-J. Koss, W. Marquardt, Direct determination of the concentration dependence of diffusivities using combined model-based Raman and NMR experiments, *Fluid Phase Equilibria*, 277 (2009), 96-106.

29. M. Člupek, P. Matějka, K. Volka, Noise Reduction in Raman spectra: Finite impulse response filtration versus Savitzky-Golay smoothing, *Journal of Raman Spectroscopy* 38 (2007), 1174-1179.

30. G. Wypych, Knovel Solvents - A Properties Database, ChemTec Publishing, 2008, (http://knovel.com/web/portal/browse/display?_EXT_KNOVEL_DISPLAY_bookid=635&VerticalID=0), 10.8.2009

31. P. S. Nikam, T. R. Mahale, M. Hasan, Density and Viscosity of Binary Mixtures of Ethyl Acetate with Methanol, Ethanol, Propan-1-ol, Propan-2-ol, Butan-1-ol, 2-Methylpropan-1-ol, and 2-Methylpropan-2-ol at (298.15, 303.15, and 308.15) K, *Journal of Chemical and Engineering data*, vol. 41, no. 5, 1996

32. J. Costa-López, A. Garvín, F. Espana, Vapor-Liquid Equilibrium Data for Methanol, Ethanol, Methyl Acetate, Ethly Acetate, and o-Xylene at 101.3 kPa, *Journal of Chemical and Engineering data*, vol. 40, no 5, 1995

33. L.S. Lee, W.C. Chen, J.F. Huang, Experiments and correlations of phase equilibria of ethanol-ethyl acetate-water ternary mixture, *Journal of Chemical Engineering of Japan*, vol. 29, no. 3, 1996

Appendix 1 Matlab code used to determine the calibration model based on the peaks heights

```
% Lappeenranta University of Technology
% Department of Chemical Technology
% Laboratory of Chemical Engineering
% Sanna Ojanen
% José Fernandes
% June 2009

% Diffusion measurements in liquid mixtures by Raman Spectroscopy

% Diffusion in binary mixtures
% of ethanol (EtOH) and ethyl acetate (EtOAc)

% Calibration model

close all;
clear all;

% molar masses, g/mol

M_EtOH = 46.07;
M_EtOAc = 88.105;

% The molar fractions in the mixtures used in the calibration

X_EtOH=[1
        0.8999
        0.8017
        0.6999
        0.6001
        0.5010
        0.4001
        0.2998
        0.1997
        0.1015
        0];

X_EtOAc=1-X_EtOH;

% masses, g

w_EtOH = X_EtOH./(X_EtOH+X_EtOAc.*(M_EtOAc/M_EtOH));

% densities in the solvent mixtures
% Ref. Nikam et al., J. Chem. Eng. Data, 41 (1996),5

roo = -0.0437*X_EtOAc.^2+0.1513*X_EtOAc+0.7861;

% concentrations, mol/cm3

c_EtOH = w_EtOH.*roo/M_EtOH;

% Load the calibration data
% Raman spectra of EtOH-Acetone mixture

% 2 accumulation and 120 sec

sol_1_a_2_120 = dlmread('EtOH_pure_a_2_120_25_06.txt');
mix_9_a_2_120 = dlmread('EtOH_EtOAc_9_a_2_120_25_06.txt');
mix_8_a_2_120 = dlmread('EtOH_EtOAc_8_a_2_120_25_06.txt');
mix_7_a_2_120 = dlmread('EtOH_EtOAc_7_a_2_120_25_06.txt');
mix_6_a_2_120 = dlmread('EtOH_EtOAc_6_a_2_120_25_06.txt');
mix_5_a_2_120 = dlmread('EtOH_EtOAc_5_a_2_120_25_06.txt');
mix_4_a_2_120 = dlmread('EtOH_EtOAc_4_a_2_120_25_06.txt');
mix_3_a_2_120 = dlmread('EtOH_EtOAc_3_a_2_120_25_06.txt');
mix_2_a_2_120 = dlmread('EtOH_EtOAc_2_a_2_120_25_06.txt');
mix_1_a_2_120 = dlmread('EtOH_EtOAc_1_a_2_120_25_06.txt');
sol_2_a_2_120 = dlmread('EtOAc_pure_a_2_120_25_06.txt');

sol_1_b_2_120 = dlmread('EtOH_pure_a_2_120_25_06.txt');
```

```
mix_9_b_2_120 = dlmread('EtOH_EtOAc_9_b_2_120_25_06.txt');
mix_8_b_2_120 = dlmread('EtOH_EtOAc_8_b_2_120_25_06.txt');
mix_7_b_2_120 = dlmread('EtOH_EtOAc_7_b_2_120_25_06.txt');
mix_6_b_2_120 = dlmread('EtOH_EtOAc_6_b_2_120_25_06.txt');
mix_5_b_2_120 = dlmread('EtOH_EtOAc_5_b_2_120_25_06.txt');
mix_4_b_2_120 = dlmread('EtOH_EtOAc_4_b_2_120_25_06.txt');
mix_3_b_2_120 = dlmread('EtOH_EtOAc_3_b_2_120_25_06.txt');
mix_2_b_2_120 = dlmread('EtOH_EtOAc_2_b_2_120_25_06.txt');
mix_1_b_2_120 = dlmread('EtOH_EtOAc_1_b_2_120_25_06.txt');
sol_2_b_2_120 = dlmread('EtOAc_pure_b_2_120_25_06.txt');

% Average for 2 accumulation and 120 sec

sol_1_2_120=(sol_1_a_2_120+sol_1_b_2_120)/2
mix_9_2_120=(mix_9_a_2_120+mix_9_b_2_120)/2
mix_8_2_120=(mix_8_a_2_120+mix_8_b_2_120)/2
mix_7_2_120=(mix_7_a_2_120+mix_7_b_2_120)/2
mix_6_2_120=(mix_6_a_2_120+mix_6_b_2_120)/2
mix_5_2_120=(mix_5_a_2_120+mix_5_b_2_120)/2
mix_4_2_120=(mix_4_a_2_120+mix_4_b_2_120)/2
mix_3_2_120=(mix_3_a_2_120+mix_3_b_2_120)/2
mix_2_2_120=(mix_2_a_2_120+mix_2_b_2_120)/2
mix_1_2_120=(mix_1_a_2_120+mix_1_b_2_120)/2
sol_2_2_120=(sol_2_a_2_120+sol_2_b_2_120)/2

%
% determine the indices of the characteristic peaks
% 2 accumulation and 120 sec

[EtOH,I]=max(sol_1_2_120(532:547,2))
I=I+531
[EtOAc,J]=max(sol_2_2_120(496:525,2))
J = J+495;

% Results:
% EtOH: 885.3030 cm-1; index 540
% EtOAc: 848.7020 cm-1; index 511

% valley points near to the characteristic peaks
% EtOH: 978.8470 cm-1; index 615
% EtOAc: 708.957 cm-1; index 402

% peak heights in all of the mixtures for EtOH

peak_EtOH_2_120= [sol_1_2_120(540,2)-sol_1_2_120(615,2)
            mix_9_2_120(540,2)-mix_9_2_120(615,2)
            mix_8_2_120(540,2)-mix_8_2_120(615,2)
            mix_7_2_120(540,2)-mix_7_2_120(615,2)
            mix_6_2_120(540,2)-mix_6_2_120(615,2)
            mix_5_2_120(540,2)-mix_5_2_120(615,2)
            mix_4_2_120(540,2)-mix_4_2_120(615,2)
            mix_3_2_120(540,2)-mix_3_2_120(615,2)
            mix_2_2_120(540,2)-mix_2_2_120(615,2)
            mix_1_2_120(540,2)-mix_1_2_120(615,2)
            sol_2_2_120(540,2)-sol_2_2_120(615,2)]

% heights of the EtOAc characteristic peaks in each mixture

peak_EtOAc_2_120= [sol_1_2_120(511,2)-sol_1_2_120(402,2)
            mix_9_2_120(511,2)-mix_9_2_120(402,2)
            mix_8_2_120(511,2)-mix_8_2_120(402,2)
            mix_7_2_120(511,2)-mix_7_2_120(402,2)
            mix_6_2_120(511,2)-mix_6_2_120(402,2)
            mix_5_2_120(511,2)-mix_5_2_120(402,2)
            mix_4_2_120(511,2)-mix_4_2_120(402,2)
            mix_3_2_120(511,2)-mix_3_2_120(402,2)
            mix_2_2_120(511,2)-mix_2_2_120(402,2)
            mix_1_2_120(511,2)-mix_1_2_120(402,2)
            sol_2_2_120(511,2)-sol_2_2_120(402,2)]

% relative height of the EtOH peak

fraction_EtOH_2_120=peak_EtOH_2_120./(peak_EtOH_2_120+peak_EtOAc_2_120)

% plot the real fraction of EtOH in the mixture as a function of
% the relative fraction of EtOH from the Raman data

figure(1);
```

```
plot(fraction_EtOH_2_120,X_EtOH,'ob')
hold off;
legend ('2 120')
xlabel('Peak height(EtOH)/(Peak height(EtOH)+Peak height(EtOAc))')
ylabel('X(EtOH))')

figure(2);
plot(fraction_EtOH_2_120,c_EtOH,'or')
hold off;
legend ('2 120')
xlabel('Peak height(EtOH)/(Peak height(EtOH)+Peak height(EtOAc))')
ylabel('c(EtOH))')

% fitting of a linear model to the calibration data
% X_EtOH = a + b * fraction_EtOH

X = [ones(length(X_EtOH),1) fraction_EtOH_2_120];
teta = X\X_EtOH;

a_2_120 = teta(1)
b_2_120 = teta(2)

%Statistic (linear)

x_l=[ones(size(fraction_EtOH_2_120(),1),1), fraction_EtOH_2_120()]; % add the '1' column
bhat_l = x_l\X_EtOH;
yhat_l = x_l*bhat_l; % the LSQ solution
res_l = X_EtOH-yhat_l; % the residuala
rss_l = sum(res_l.^2); % the residual sum of squares
s2_l = rss_l/(11-2); % the variance of noise in y
cb_l = inv(x_l'*x_l)*s2_l; % covariance of b
sdb_l = sqrt(diag(cb_l)); % the standard deviations of
tb_l = bhat_l./sdb_l; % the t-values
tss_l = sum((X_EtOH-mean(X_EtOH)).^2); % the total sum of squares
R2_l = 1-rss_l/tss_l; % R^2 value

% fitting of a quadractic model to the calibration data
% X_EtOH = a + b * fraction_EtOH + c * fraction_EtOH

X_x = [ones(length(X_EtOH),1) fraction_EtOH_2_120  fraction_EtOH_2_120.^2];
teta = X_x\X_EtOH;

a_x_2_120 = teta(1)
b_x_2_120 = teta(2)
c_x_2_120 = teta(3)

%statistic (quadractic)

x=[ones(size(fraction_EtOH_2_120(),1),1), fraction_EtOH_2_120(), fraction_EtOH_2_120().^2]; %
add the '1' column
bhat = x\X_EtOH;
yhat = x*bhat; % the LSQ solution
res = X_EtOH-yhat; % the residuala
rss = sum(res.^2); % the residual sum of squares
s2 = rss/(11-2); % the variance of noise in y
cb = inv(x'*x)*s2; % covariance of b
sdb = sqrt(diag(cb)); % the standard deviations of
tb = bhat./sdb; % the t-values
tss = sum((X_EtOH-mean(X_EtOH)).^2); % the total sum of squares
R2 = 1-rss/tss; % R^2 value
```

Appendix 2 Matlab code used to determine the calibration model based on the area under the peaks

```
% Lappeenranta University of Technology
% Department of Chemical Technology
% Laboratory of Chemical Engineering
% Sanna Ojanen
% José Fernandes
% July 2009


% Diffusion measurements in liquid mixtures by Raman Spectroscopy

% Diffusion in binary mixtures
% of ethanol (EtOH) and ethyl acetate (EtOAc)

% Calibration model

close all;
clear all;

% molar masses, g/mol

M_EtOH = 46.07;
M_EtOAc = 88.105;

% The molar fractions in the mixtures used in the calibration

X_EtOH=[1
        0.8999
        0.8017
        0.6999
        0.6001
        0.5010
        0.4001
        0.2998
        0.1997
        0.1015
        0];

X_EtOAc=1-X_EtOH;

% masses, g

w_EtOH = X_EtOH./(X_EtOH+X_EtOAc.*(M_EtOAc/M_EtOH));

% densities in the solvent mixtures
% Ref. Nikam et al., J. Chem. Eng. Data, 41 (1996),5

roo = -0.0437*X_EtOAc.^2+0.1513*X_EtOAc+0.7861;

% concentrations, mol/cm3

c_EtOH = w_EtOH.*roo/M_EtOH;


%% Load the calibration data
% Raman spectra of EtOH-Acetone mixture
% 2 accumulation and 120 sec

sol_1_a_2_120 = dlmread('EtOH_pure_a_2_120_25_06.txt');
mix_9_a_2_120 = dlmread('EtOH_EtOAc_9_a_2_120_25_06.txt');
mix_8_a_2_120 = dlmread('EtOH_EtOAc_8_a_2_120_25_06.txt');
mix_7_a_2_120 = dlmread('EtOH_EtOAc_7_a_2_120_25_06.txt');
mix_6_a_2_120 = dlmread('EtOH_EtOAc_6_a_2_120_25_06.txt');
mix_5_a_2_120 = dlmread('EtOH_EtOAc_5_a_2_120_25_06.txt');
mix_4_a_2_120 = dlmread('EtOH_EtOAc_4_a_2_120_25_06.txt');
mix_3_a_2_120 = dlmread('EtOH_EtOAc_3_a_2_120_25_06.txt');
```

```
mix_2_a_2_120 = dlmread('EtOH_EtOAc_2_a_2_120_25_06.txt');
mix_1_a_2_120 = dlmread('EtOH_EtOAc_1_a_2_120_25_06.txt');
sol_2_a_2_120 = dlmread('EtOAc_pure_a_2_120_25_06.txt');

sol_1_b_2_120 = dlmread('EtOH_pure_a_2_120_25_06.txt');
mix_9_b_2_120 = dlmread('EtOH_EtOAc_9_b_2_120_25_06.txt');
mix_8_b_2_120 = dlmread('EtOH_EtOAc_8_b_2_120_25_06.txt');
mix_7_b_2_120 = dlmread('EtOH_EtOAc_7_b_2_120_25_06.txt');
mix_6_b_2_120 = dlmread('EtOH_EtOAc_6_b_2_120_25_06.txt');
mix_5_b_2_120 = dlmread('EtOH_EtOAc_5_b_2_120_25_06.txt');
mix_4_b_2_120 = dlmread('EtOH_EtOAc_4_b_2_120_25_06.txt');
mix_3_b_2_120 = dlmread('EtOH_EtOAc_3_b_2_120_25_06.txt');
mix_2_b_2_120 = dlmread('EtOH_EtOAc_2_b_2_120_25_06.txt');
mix_1_b_2_120 = dlmread('EtOH_EtOAc_1_b_2_120_25_06.txt');
sol_2_b_2_120 = dlmread('EtOAc_pure_b_2_120_25_06.txt');

% Average for 2 accumulation and 120 sec

sol_1_2_120=(sol_1_a_2_120+sol_1_b_2_120)/2
mix_9_2_120=(mix_9_a_2_120+mix_9_b_2_120)/2
mix_8_2_120=(mix_8_a_2_120+mix_8_b_2_120)/2
mix_7_2_120=(mix_7_a_2_120+mix_7_b_2_120)/2
mix_6_2_120=(mix_6_a_2_120+mix_6_b_2_120)/2
mix_5_2_120=(mix_5_a_2_120+mix_5_b_2_120)/2
mix_4_2_120=(mix_4_a_2_120+mix_4_b_2_120)/2
mix_3_2_120=(mix_3_a_2_120+mix_3_b_2_120)/2
mix_2_2_120=(mix_2_a_2_120+mix_2_b_2_120)/2
mix_1_2_120=(mix_1_a_2_120+mix_1_b_2_120)/2
sol_2_2_120=(sol_2_a_2_120+sol_2_b_2_120)/2

wave = sol_1_2_120(:,1);
intensity = [sol_1_2_120(:,2)'
             mix_9_2_120(:,2)'
             mix_8_2_120(:,2)'
             mix_7_2_120(:,2)'
             mix_6_2_120(:,2)'
             mix_5_2_120(:,2)'
             mix_4_2_120(:,2)'
             mix_3_2_120(:,2)'
             mix_2_2_120(:,2)'
             mix_1_2_120(:,2)'
             sol_2_2_120(:,2)'];

%% area under the peaks

%EtOH peak

intens1_0=intensity(:,525:556);
wave1=wave(525:556)
intens1_min=min(intens1_0,[],2);
for p=1:length(intens1_min)%each spectrum
    intens1_dif(p,:)=intens1_0(p,:)-intens1_min(p);%for interpolation this is intens1_dif
    size(wave1)
    size(intens1_dif(p,:))
    length(intens1_min)
     intens1(p,:)=interp1(wave1',intens1_dif(p,:),867:0.2:904,'pchip',0);
    for k=2:(length(wave1)-1)
        A1k(p,k)=abs(wave1(k+1)-wave1(k))*intens1(p,k)+0.5*abs(wave1(k+1)-
wave1(k))*abs(intens1(p,k+1)-intens1(p,k));
    end
    A1(p)=sum(A1k(p,:));

end

%EtOAc peak

intens2_0=intensity(:,499:523);
wave2=wave(499:523);
intens2_min=min(intens2_0,[],2);
for p=1:length(intens2_min)
    intens2_dif(p,:)=intens2_0(p,:)-intens2_min(p);
    size(wave2)
    size(intens2_dif(p,:))
  intens2(p,:)=interp1(wave2',intens2_dif(p,:),835:0.2:860,'pchip',0);
    for k=2:(length(wave2)-1)
        A2k(p,k)=abs(wave2(k+1)-wave2(k))*intens2(p,k)+0.5*abs(wave2(k+1)-
wave2(k))*abs(intens2(p,k+1)-intens2(p,k));
    end
```

```
    A2(p)=sum(A2k(p,:));

end


figure('Name','Peak1','NumberTitle','off')
subplot(2,1,1)
size(wave1)
size(intens1)
plot(867:0.2:904,intens1)
xlabel('Wave [cm^-1]')
ylabel('Intensity [a.u.]')
title('Intensity as a function of wave lenght for 1st component')
legend('EtOH','5','4','3','2','1','EtOAc')
subplot(2,1,2)
plot(X_EtOH,A1,'*')
xlabel('Molar fraction of EtOH, -')
ylabel('Area under the peak')
title('Area under the peak for all spectrum')


figure('Name','Peak2','NumberTitle','off')
subplot(2,1,1)
size(wave2)
size(intens2)
plot(835:0.2:860,intens2)
xlabel('Wave  [cm^-1]')
ylabel('Intensity [a.u.]')
title('Intensity as a function of wave lenght for 2nd component')
subplot(2,1,2)
plot(X_EtOH,A2,'*')
xlabel('Molar fraction of EtOH')
ylabel('Area under the peak')
title('Area under the peak for all spectrum')

%% areas ratio for each spectrum
% ratio of the two peaks
var= abs(A1./(A1+A2));

figure('Name','Fraction','NumberTitle','off');
plot(var,X_EtOH,'ok')
xlabel('EtOH peak area ratio')
ylabel('EtOH molar fraction')

% fitting of a linear model to the calibration data
% X_EtOH = a + b * var

X_area = [ones(length(X_EtOH),1) var()']
teta = X_area\X_EtOH();

a_area = teta(1)
b_area = teta(2)

%Statistic (linear)

x=[ones(size(var()',1),1), var()']; % add the '1' column
bhat = x\X_EtOH;
yhat = x*bhat; % the LSQ solution
res = X_EtOH-yhat; % the residuala
rss = sum(res.^2); % the residual sum of squares
s2 = rss/(11-2); % the variance of noise in y
cb = inv(x'*x)*s2; % covariance of b
sdb = sqrt(diag(cb)); % the standard deviations of
tb = bhat./sdb; % the t-values
tss = sum((X_EtOH-mean(X_EtOH)).^2); % the total sum of squares
R2 = 1-rss/tss; % R^2 value


% fitting of a linear model to the calibration data
% X_EtOH = a + b * fraction_EtOH + c * fraction_EtOH

X_x = [ones(length(X_EtOH),1) var()'  var()'.^2];
teta = X_x\X_EtOH;

a_x_2_120 = teta(1)
b_x_2_120 = teta(2)
c_x_2_120 = teta(3)
```

```
%statistic (quadractic)

x_1=[ones(size(var()',1),1), var()', var()'.^2]; % add the '1' column
bhat_1 = x_1\X_EtOH;
yhat_1 = x_1*bhat_1; % the LSQ solution
res_1 = X_EtOH-yhat_1; % the residuala
rss_1 = sum(res_1.^2); % the residual sum of squares
s2_1 = rss_1/(11-2); % the variance of noise in y
cb_1 = inv(x_1'*x_1)*s2_1; % covariance of b
sdb_1 = sqrt(diag(cb_1)); % the standard deviations of
tb_1 = bhat_1./sdb_1; % the t-values
tss_1 = sum((X_EtOH-mean(X_EtOH)).^2); % the total sum of squares
R2_1 = 1-rss_1/tss_1; % R^2 value
```

Appendix 3 Matlab code used to determine the diffusivities and the diffusion profiles using the model based on the peaks heights

```
% Lappeenranta University of Technology
% Department of Chemical Technology
% Laboratory of Chemical Engineering
% Sanna Ojanen
% José Fernandes
% June 2009


% Diffusion measurements in liquid mixtures by Raman Spectroscopy

% Diffusion in binary mixtures
% of ethanol (EtOH) and ethyl acetate (EtOAc)

close all;
clear all;

% volumes of the two phases, mL

Vupper = 10;
Vlower = 9;

% height of the measurement point, mL
% from the initial boundary

Vobs = 12;

% scale transformation
% cylinder, d = 2 cm

r = 0.01;

L = (Vupper+Vlower)/(1000000*pi()*r^2);
x_probe = Vobs/(1000000*pi()*r^2);
x_ib = Vlower/(1000000*pi()*r^2);
z = x_probe-x_ib;

% Properties of the solvents
% EtOH = 1
% EtOAc = 2

% molar masses, g/mol

M1 = 46.07;
M2 = 88.105;

% densities, g/cm3

roo1 = 0.78517;
roo2 = 0.8948;

% molar volumes, cm3/mol

Vm1 = M1/roo1;
Vm2 = M2/roo2;


% initial compositions of the two phases

% molar fractions, -
x1upper = 0.5005;
x1lower = 0.2995;
x2upper = 1-x1upper;
x2lower = 1-x1lower;

% mass fractions, -
```

```
w1upper = x1upper/(x1upper+x2upper*(M2/M1));
w1lower = x1lower/(x1lower+x2lower*(M2/M1));
w2upper = 1-w1upper;
w2lower= 1-w1lower;

% densities of the initial phases, g/cm3
rooupper = -0.0437*x2upper.^2+0.1513*x2upper+0.7861;
roolower = -0.0437*x2lower.^2+0.1513*w2lower+0.7861;

% masses of the initial phases, g
mupper = rooupper*Vupper;
mlower = roolower*Vlower;

% molar amount, mol
n1upper = (mupper*w1upper)/M1;
n1lower = (mlower*w1lower)/M1;
n2upper = (mupper*w2upper)/M2;
n2lower = (mlower*w2lower)/M2;

ntotal = n1upper+n2upper+n1lower+n2lower;

% initial concentrations

c1upper = n1upper/Vupper;
c2upper = n2upper/Vupper;
c1lower = n1lower/Vlower;
c2lower = n2lower/Vlower;

% average molar fraction, -
x1_avg = (n1upper+n1lower)/ntotal;
x2_avg = (n2upper+n2lower)/ntotal;

% average concentration, mol/cm3
c1_avg = (n1upper+n1lower)/(Vupper+Vlower);
c2_avg = (n2upper+n2lower)/(Vupper+Vlower);

% load the data
data = dlmread('EtOH_EtOAc_24h_1_d_2_120_multi_simple_26_06.txt');

% size of the data matrix (rows, columns
matsize = size(data);

% wave numbers are given in the first row of the data matrix
% the first two numbers are missing

wave = data(1,1:(matsize(2)-1));

% intensities
% the first row (wave numbers) is removed
% the first two columns are removed, too

intensity = data(2:matsize(1),2:matsize(2));

% plot the spectral data

% figure(1);
% plot(wave,intensity)
% ylabel('intensity, a.u.')
% xlabel('wavenumber, cm-1')

% the injection time, s
% starting point of the measurement

time0 = 250;

% time interval between the measurements (step size), s

step = 300;

%% check the peak heights etc. for each spectrum

for i = 1:(matsize(1)-1)

    % the characteristic peak of compound 1 (EtOH)
    % peak: 887,746 cm-1; index 542
    % valley 965,156 cm-1; index 604
    pk1(i) = intensity(i,542)-intensity(i,604);
```

```
    % the characteristic peak of compound 2 (EtOAc)
    % peak 849,896 cm-1; index 512
    % valley 818,157 cm-1; index 487
    pk2(i) = intensity(i,512)-intensity(i,487);

    % ratio of the two peaks
    var(i)= pk1(i)/(pk1(i)+pk2(i));

   % the molar fraction of component 1
    % based on the calibration model
    % y = b*x+a
    frac1(i) = -0.2026*var(i)^2+1.1960*var(i)+0.0177;
    %frac1(i) = 1.0022*var(i)+0.0439;
    frac2(i) = 1-frac1(i);

    % the concentration of component 1
    % based on the calibration model
    % y = c*x^2+b*x+a
    conc1(i) = 0.0057*var(i)^2+0.0114*var(i)+2.5458E-4;

    % measurement time point

    time (i) = time0+(i-1)*step;

end
%% 3D Spectrums

% 3D, 289 spectrums (all)
figure();
wave=wave(450:600);
intensity=intensity(:,450:600);
for i=1:289
    A=[wave(:) intensity(i,:)'];
    s=ones(size(A(:,1)));
    line(s*time(1,i),A(:,1),A(:,2))
end

% 3D figure, each spectrum is a average of 10 or 9 spectrum
figure();
intensity_a=intensity;
intensity_b=[sum(intensity_a(1:10,:))/10
    sum(intensity_a(11:20,:))/10
    sum(intensity_a(21:30,:))/10
    sum(intensity_a(31:40,:))/10
    sum(intensity_a(41:50,:))/10
    sum(intensity_a(51:60,:))/10
    sum(intensity_a(61:70,:))/10
    sum(intensity_a(71:80,:))/10
    sum(intensity_a(81:90,:))/10
    sum(intensity_a(91:100,:))/10
    sum(intensity_a(101:110,:))/10
    sum(intensity_a(111:120,:))/10
    sum(intensity_a(121:130,:))/10
    sum(intensity_a(131:140,:))/10
    sum(intensity_a(141:150,:))/10
    sum(intensity_a(151:160,:))/10
    sum(intensity_a(161:170,:))/10
    sum(intensity_a(171:180,:))/10
    sum(intensity_a(181:190,:))/10
    sum(intensity_a(191:200,:))/10
    sum(intensity_a(201:210,:))/10
    sum(intensity_a(211:220,:))/10
    sum(intensity_a(221:230,:))/10
    sum(intensity_a(231:240,:))/10
    sum(intensity_a(241:250,:))/10
    sum(intensity_a(251:260,:))/10
    sum(intensity_a(261:270,:))/10
    sum(intensity_a(271:280,:))/10
    sum(intensity_a(281:289,:))/9];

time_plot=time(1:29)*10;
intensity_plot=intensity_b(1:29,:);
waterfall(wave,time_plot,intensity_plot)
%% Evolution of the molar fraction, concentration and peak heights

figure(2);

% plot the change in the molar fraction of 1 as a function of time
```

```
subplot(3,1,1);
x1final = x1_avg*ones(length(time));
plot(time,frac1,'b',time,x1final,'g')
legend('measured','final')
title('molar fraction of EtOH')
% plot the change in the concentration of 1 as a function of time
subplot(3,1,2);
c1final = c1_avg*ones(length(time));
plot(time,conc1,'r',time,c1final,'g')
legend('measured','final')
title('concentration of EtOH')
% plot the peak heights
subplot(3,1,3);
plot(time,pk1,time,pk2)
title('peak heights')
legend('EtOH','EtOAc')
xlabel('time, s')

%% animation showing the change in the two characteristic peaks

% plots the spectra around the characteristic peaks only
% (not the whole wavenumber range)

% the axis will be fixed

xmin = 820;
xmax = 905;
ymin = 100;
ymax = 9000;

figure(3);
ylabel('intensity, a.u.')
xlabel('wavenumber, cm-1')
for k = 1:(matsize(1)-1)
    plot(wave(:),intensity(k,:))
    axis([xmin,xmax,ymin,ymax])
    ylabel('intensity, a.u.')
    xlabel('wavenumber, cm-1')
    title(time(k))
    % the rate of changing the figure
    pause(.0333)

end


%% Determination of the diffusion coefficient D
% for EtOAc in EtOH
% based on Fick's 2nd law
D = 1e-9;
%L = 0.06;  % length of spatial interval (total height of the liquids)
param = [D L];

% discretization
n     = 200;              % n of spatial discretization
x     = linspace(0,L,n); % discretization points
tspan = linspace(0,2000000,1000); %time points for solution
tspan = [tspan 10000000];      %(add one more time point for steady state!)


% measurement point
% x_probe = 0.04;
x_probe = x_ib + 0.008;
iobs = max(find(x<x_probe));
%x_ib = x_probe-z; % initial boundary level from the bottom of the cell

% initial values, a step function
c0     = x2upper*ones(n,1);
i1     = find(x<x_ib);
ni = length(i1);
c0(i1) = x2lower*ones(ni,1);


% initial quess for D, cm2/s

D_init = 1E-9;

data = [time' frac2'];
const(1) = L;
```

```
const(2) = iobs;

% call the lsq function
D_opt = fminsearch(@lsq_diff,D_init,[],c0,data,const) % m2/s

param = [D_opt L];

tic;
[t,c]=ode15s(@difff,tspan,c0,[],param);
cputime = toc;

% plot the diffusion profile in the cell
figure(4);
plot(x,c)
axis([0,L,x2upper,x2lower])

% molar fractions of EtOAc
% calculated using the obtained D value
% based on Fick's 2nd law

z = 0.008;

init_D = D_opt;

D_opt_inf = fminsearch('diffusion',init_D,[],x2lower,x2upper,time,z,frac2)

frac2mod = (x2lower+x2upper)/2-((x2lower-x2upper)/2)*erf(z./(2*sqrt(D_opt_inf*t(2:end))));
frac2mod = [x2upper
            frac2mod];
%check the mass conservation

dx   = x(2)-x(1);
mass = sum(c'*dx);
%figure(6);
x2final = x2_avg*ones(size(t));
x2initial = x2upper*ones(size(t));

% plot the computed observation value
% and the measurement data
% concentration - time profile at height z
figure(5);
y_comp = c(:,iobs);
t_h = t./3600;
time_h = time./3600;
plot(t_h,y_comp,'-b',time_h,frac2,'ok',t_h,frac2mod,'-r',t_h,x2final,'-k',t_h,x2initial,'-k')
hold on;

legend('model','experiment','analytical','final & initial')
ylabel('molar fraction of 2, -')
xlabel('time, h')
%plot(tspan, mass,'.-');
```

Appendix 4 Matlab code used to determine the diffusivities and the diffusion profiles using the model based on areas under the peaks

```
% Lappeenranta University of Technology
% Department of Chemical Technology
% Laboratory of Chemical Engineering
% Sanna Ojanen
% José Fernandes
% July 2009


% Diffusion measurements in liquid mixtures by Raman Spectroscopy

% Diffusion in binary mixtures
% of ethanol (EtOH) and ethyl acetate (EtOAc)

clc;
close all;
clear all;


% volumes of the two phases, mL

Vupper = 10;
Vlower = 9;

% height of the measurement point, mL
% from the initial boundary

Vobs = 12;

% scale transformation
% cylinder, d = 2 cm

r = 0.01;

L = (Vupper+Vlower)/(1000000*pi()*r^2);
x_probe = Vobs/(1000000*pi()*r^2);
x_ib = Vlower/(1000000*pi()*r^2);
z = x_probe-x_ib;


% Properties of the solvents
% EtOH = 1
% EtOAc = 2

% molar masses, g/mol

M1 = 46.07;
M2 = 88.105;

% densities, g/cm3

roo1 = 0.78517;
roo2 = 0.8948;

% molar volumes, cm3/mol

Vm1 = M1/roo1;
Vm2 = M2/roo2;


% initial compositions of the two phases

% molar fractions,
x1upper = 0.5005;
x1lower = 0.2995;
x2upper = 1-x1upper;
```

```
x2lower = 1-x1lower;

% mass fractions, -
w1upper = x1upper/(x1upper+x2upper*(M2/M1));
w1lower = x1lower/(x1lower+x2lower*(M2/M1));
w2upper = 1-w1upper;
w2lower= 1-w1lower;

% densities of the initial phases, g/cm3
rooupper = -0.0437*x2upper.^2+0.1513*x2upper+0.7861;
roolower = -0.0437*x2lower.^2+0.1513*w2lower+0.7861;

% masses of the initial phases, g
mupper = rooupper*Vupper;
mlower = roolower*Vlower;

% molar amount, mol
n1upper = (mupper*w1upper)/M1;
n1lower = (mlower*w1lower)/M1;
n2upper = (mupper*w2upper)/M2;
n2lower = (mlower*w2lower)/M2;

ntotal = n1upper+n2upper+n1lower+n2lower;

% initial concentrations

c1upper = n1upper/Vupper;
c2upper = n2upper/Vupper;
c1lower = n1lower/Vlower;
c2lower = n2lower/Vlower;

% average molar fraction, -
x1_avg = (n1upper+n1lower)/ntotal;
x2_avg = (n2upper+n2lower)/ntotal;

% average concentration, mol/cm3
c1_avg = (n1upper+n1lower)/(Vupper+Vlower);
c2_avg = (n2upper+n2lower)/(Vupper+Vlower);

% load the data
data = dlmread('EtOH_EtOAc_24h_1_d_2_120_multi_simple_26_06.txt');

% size of the data matrix (rows, columns)
matsize = size(data);

% wave numbers are given in the first row of the data matrix
% the first two numbers are missing
wave = data(1,1:(matsize(2)-2));

% intensities
% the first row (wave numbers) is removed
% the first two columns are removed, too
intensity = data(2:matsize(1),3:matsize(2));

% the injection time, s
% starting point of the measurement
time0 = 250;

% time interval between the measurements (step size), s
step = 300;

%% plot the spectral data
figure;
plot(wave,intensity)
ylabel('intensity, a.u.')
xlabel('wavenumber, cm-1')

%% area under the peaks

% EtOH peak

intens1_0=intensity(:,525:556);
wave1=wave(525:556);
intens1_min=min(intens1_0,[],2);
for p=1:length(intens1_min)%each spectrum
    intens1_dif(p,:)=intens1_0(p,:)-intens1_min(p);%for interpolation this is intens1_dif
    size(wave1)
    size(intens1_dif(p,:))
```

```
    length(intens1_min)
    %for p=1:length(intens1_min)
    intens1(p,:)=interp1(wave1,intens1_dif(p,:),867:0.2:904,'pchip',0);
    %end
    for k=1:(length(wave1)-1)
        A1k(p,k)=abs(wave1(k+1)-wave1(k))*intens1(p,k)+0.5*(wave1(k+1)-
wave1(k))*abs(intens1(p,k+1)-intens1(p,k));
    end
    A1(p)=sum(A1k(p,:));
end

% EtOAc peak

intens2_0=intensity(:,499:523);
wave2=wave(499:523);
intens2_min=min(intens2_0,[],2);
for p=1:length(intens1_min)
    intens2_dif(p,:)=intens2_0(p,:)-intens2_min(p);
    size(wave2)
    size(intens2_dif(p,:))
    length(intens2_min)
    intens2(p,:)=interp1(wave2,intens2_dif(p,:),835:0.2:860,'pchip',0);
    for k=1:(length(wave2)-1)
        A2k(p,k)=abs(wave2(k+1)-wave2(k))*intens2(p,k)+0.5*(wave2(k+1)-
wave2(k))*abs(intens2(p,k+1)-intens2(p,k));
    end
    A2(p)=sum(A2k(p,:));


end
%%
figure('Name','Peak1','NumberTitle','off')
subplot(2,1,1)
size(wave1)
size(intens1)
plot(867:0.2:904,intens1)
%subplot(2,1,1),plot(wave1,intens1)
xlabel('Wave [cm^-1]')
ylabel('Intensity [a.u.]')
title('Intensity as a function of wave lenght for first component')
subplot(2,1,2),plot(A1,'*')
xlabel('spectrum number')
ylabel('Area under the peak [a.u.*cm^-1]')
title('Area under the peak for all spectrum')

figure('Name','peak2','NumberTitle','off')
subplot(2,1,1)
size(wave2)
size(intens2)
plot(835:0.2:860,intens2)
%subplot(2,1,1),plot(wave2,intens2)
xlabel('Wave  [cm^-1]')
ylabel('Intensity [a.u.]')
title('Intensity as a function of wave lenght for first component')
subplot(2,1,2),plot(A2,'*')
xlabel('spectrum number')
ylabel('Area under the peak [a.u.*cm^-1]')
title('Area under the peak for all spectrum')

%% areas ratio for each spectrum

for i = 1:(matsize(1)-1)
      % ratio of the two peaks
    var(i)=abs( A1(i)/(A1(i)+A2(i)));
    % the molar fraction of component 1
    % based on the calibration model
    %y=b*x+a
    %the spectra of pure solvents included in the model
    %frac1(i) = -0.31*var(i)^2+1.9*var(i)-0.54;
    frac1(i)=1.5*var(i)-0.43
    frac2(i) = 1-frac1(i);
    time (i) = time0+(i-1)*step;
end

%%
figure;
% plot the change in the molar fraction of 1 as a function of time
subplot(2,1,1);
```

```
x1final = x1_avg*ones(length(time));
plot(time,frac1,'b',time,x1final,'g')
legend('measured','final')
title('molar fraction of EtOH')
subplot(2,1,2);
plot(time,A1,time,A2)
title('peak Areas')
legend('EtOH','EtOAc')
xlabel('time, s')

%% animation showing the change in the two characteristic peaks

% plots the spectra around the characteristic peaks only
% (not the whole wavenumber range)

% the axis will be fixed

xmin = 800;
xmax = 920;
ymin = 100;
ymax = 9500;

figure;
ylabel('intensity, a.u.')
xlabel('wavenumber, cm-1')
for k = 1:(matsize(1)-1)
    plot(wave(380:580),intensity(k,380:580))
%     hold on
    axis([xmin,xmax,ymin,ymax])
    ylabel('intensity, a.u.')
    xlabel('wavenumber, cm-1')
    title(time(k))
    %the rate of changing the figure
    pause(.0000333)
end

%% Determination of the diffusion coefficient D
% for EtOAc in EtOH
% based on Fick's 2nd law
D = 1e-9;
%L = 0.06;  % length of spatial interval (total height of the liquids)
param = [D L];

% discretization
n     = 200;              % n of spatial discretization
x     = linspace(0,L,n);  % discretization points
tspan = linspace(0,2000000,1000); %time points for solution
tspan = [tspan 10000000];      %(add one more time point for steady state!)


% measurement point
% x_probe = 0.04;
x_probe = x_ib + 0.008;
iobs = max(find(x<x_probe));
%x_ib = x_probe-z; % initial boundary level from the bottom of the cell

% initial values, a step function
c0     = x2upper*ones(n,1);
i1     = find(x<x_ib);
ni = length(i1);
c0(i1) = x2lower*ones(ni,1);

% initial quess for D, cm2/s

D_init = 1E-9;

data = [time' frac2'];
const(1) = L;
const(2) = iobs;

% call the lsq function
D_opt = fminsearch(@lsq_diff,D_init,[],c0,data,const) % m2/s

param = [D_opt L];

tic;
[t,c]=ode15s(@difff,tspan,c0,[],param);
cputime = toc;
```

```
% plot the diffusion profile in the cell
figure;
plot(x,c)
axis([0,L,x2upper,x2lower])
title('Cell profile')

% molar fractions of EtOAc
% calculated using the obtained D value
% based on Fick's 2nd law

z = 0.008;

init_D = D_opt;

D_opt_inf = fminsearch('diffusion',init_D,[],x2lower,x2upper,time,z,frac2)

frac2mod = (x2lower+x2upper)/2-((x2lower-x2upper)/2)*erf(z./(2*sqrt(D_opt_inf*t(2:end))));
frac2mod = [x2upper
    frac2mod];
%check the mass conservation

dx   = x(2)-x(1);
mass = sum(c'*dx);
%figure(6);
x2final = x2_avg*ones(size(t));
x2initial = x2upper*ones(size(t));

% plot the computed observation value
% and the measurement data
% concentration - time profile at height z

figure;
y_comp = c(:,iobs);
t_h = t./3600;
time_h = time./3600;
plot(t_h,y_comp,'-b',time_h,frac2,'ok',t_h,frac2mod,'-r',t_h,x2final,'-k',t_h,x2initial,'-k')
hold on;
legend('model','experiment','analytical','final & initial')
ylabel('molar fraction of 2, -')
xlabel('time, h')
%plot(tspan, mass,'.-');
```

Appendix 5 Functions used in the determination of the analytical and the numeric solutions

```
function dc = difff(t,c,param);
%INPUT   t      time point
%        c      the solution at t
%        param  model parametes
%OUTPUT  dc     the time derivative of A at time t

%parameters
D = param(1);
L = param(2);
n = length(c);
%BC
 cx = zeros(n,1);
 nl = 2;  %boundary condition (zero derivative given)
 nu = 2;  % -  " -
%2. derivatives
 cxx= dss044(0,L,c,cx,nl,nu);

 dc =  D*cxx;


function ss = diffusion(D,x2lower,x2upper,time,z,frac2)

% molar fraction of component 2
% using Fick's 2nd law and diffusion coefficient D

frac2calc = (x2lower+x2upper)/2-((x2lower-x2upper)/2)*erf(z./(2*sqrt(D*time')));

% least squares function to be minimized
ss = sum((frac2'-frac2calc).^2);


function ss = lsq_diff(D,c0,data,const);

t_obs = data(:,1);
y_obs = data(:,2);

L = const(1); %length of spatial interval
iobs = const(2);

param = [D L];

[t,c]=ode15s(@difff,t_obs,c0,[],param);

y_comp = c(:,iobs);
ss = sum((y_obs-y_comp).^2);
```